HHS Public Access

Author manuscript

Dev Dyn. Author manuscript; available in PMC 2024 February 05.

Published in final edited form as:

Dev Dyn. 2024 January ; 253(1): 119–143. doi:10.1002/dvdy.652.

SMAD4: A Critical Regulator of Cardiac Neural Crest Cell Fate and Vascular Smooth Muscle Development

Brianna E. Alexander[1,2,#], **Huaning Zhao**[1,#], **Sophie Astrof**[1,2,3,*]

[1.]Department of Cell Biology and Molecular Medicine, New Jersey Medical School, Rutgers Biomedical and Health Sciences, Newark, NJ, 07103

[2.]Multidisciplinary Ph.D. Program in Biomedical Sciences: Cell Biology, Neuroscience and Physiology Track, New Jersey Medical School, Rutgers Biomedical and Health Sciences, Newark, NJ, 07103

[3.]Multidisciplinary Ph.D. Program in Biomedical Sciences: Molecular Biology, Genetics, and Cancer Track, New Jersey Medical School, Rutgers Biomedical and Health Sciences, Newark, NJ, 07103

Abstract

Background: During embryogenesis, cardiac neural crest-derived cells (NCs) migrate into the pharyngeal arches and give rise to the vascular smooth muscle cells (vSMCs) of the pharyngeal arch arteries (PAAs). vSMCs are critical for the remodeling of the PAAs into their final adult configuration, giving rise to the aortic arch and its arteries (AAAs).

Results: We investigated the role of SMAD4 in NC-to-vSMC differentiation using lineage-specific inducible mouse strains. We found that the expression of SMAD4 in the NC is indelible for regulating the survival of cardiac NCs. Although the ablation of SMAD4 at E9.5 in the NC lineage led to a near-complete absence of NCs in the pharyngeal arches, PAAs became invested with vSMCs derived from a compensatory source. Analysis of AAA development at E16.5 showed that the alternative vSMC source compensated for the lack of NC-derived vSMCs and rescued AAA morphogenesis.

Conclusions: Our studies uncovered the requisite role of SMAD4 in the contribution of the NC to the pharyngeal arch mesenchyme. We found that in the absence of $SMAD4^{+}$ NCs, vSMCs around the PAAs arose from a different progenitor source, rescuing AAA morphogenesis. These findings shed light on the remarkable plasticity of developmental mechanisms governing AAA development.

1. Introduction

The cardiovascular system is the first organ system formed during embryonic development [1,2]. Defects affecting the heart and/or its associated vasculature are collectively termed Congenital Heart Disease (CHD). CHD is one of the most common human birth defects, affecting ~1% of all live births annually [3]. It is also the primary cause of infant mortality,

*Author for correspondence, Sophie Astrof (sophie.astrof@rutgers.edu).
#These authors contributed equally to the article.

with an estimated 25% of all CHD cases so severe, termed “critical CHDs,” that they necessitate surgical intervention immediately after birth [4-6]. Longitudinal studies revealed that while 82.5% of all critical CHD patients survive to 1 year, only 68.8% survive to adulthood (18 years of age) [4]. Despite these staggering statistics, only a reported 15% of all CHD cases are linked to a known cause, underscoring the need to elucidate the etiology of CHD so that new diagnostic, preventative, and treatment options can be developed [7].

Among critical CHDs are phenotypes affecting the aortic arch arteries (AAAs), the vessels which connect to the aortic arch and route oxygenated blood into the systemic circulation. Any occlusion or malformation of these vessels disrupts blood flow throughout the body demanding urgent surgical intervention for survival [8,9]. During embryogenesis, the AAAs originate from three pairs of symmetrical vessels, the 3rd, 4th, and 6th pharyngeal arch arteries (PAAs), also called the carotid, aortic, and pulmonary arteries [10]. These arteries undergo asymmetrical remodeling (between E11.5-E13.5 in murine embryos) to form the AAA tree [11,12]. PAA-to-AAA remodeling is facilitated by the cardiac neural crest (NC) cells. Cardiac NCs are a subset of cranial NCs. Cardiac NCs that migrate into the outflow tract are necessary for the development of the aorticopulmonary septum and aortic valves. Cardiac NCs that migrate into the posterior pharyngeal arches (3-6) give rise to the vascular smooth muscle cells (vSMCs) around the 3rd, 4th, and 6th PAAs, facilitating PAA stability and the remodeling of the symmetrical PAAs into the asymmetric AAA tree [13,14].

In the 3rd - 6th pharyngeal arches, cardiac NCs form several cell layers around the second heart field-derived endothelium of the PAAs [14,15]. NCs closest to the endothelium differentiate into vSMCs [14,16,17]. NC-to-vSMC differentiation is critical to proper AAA morphogenesis as it enables the developing vessel to maintain physical integrity under the forces of blood flow and vascular remodeling [14,18,19]. Processes that interfere with NC development in the pharyngeal region, including NC migration, vSMC differentiation, or NC survival, can result in arch artery regression and critical CHD [17]. The left 4th PAA gives rise to the arch of the aorta. Given the severity of the 4th PAA-related phenotypes, we focused our studies on the development of NCs surrounding the 4th PAAs.

Genetic mutations have been implicated in cardiovascular phenotypes in CHD, including *JAG1*, linked to Alagille syndrome, *CHD7*, linked to CHARGE syndrome, *TBX1*, linked to 22q11.2 syndrome, [20] and recently SMAD4, linked to Myhre syndrome [21,22]. SMAD4 is the common signaling component in the canonical TGFβ and BMP signaling pathways. In addition to its role as a tumor suppressor [23,24], SMAD4 is known to be critical for proper gastrulation and embryonic development. Global SMAD4-null mutants are embryonic lethal by E8.5 due to improper development of the mesoderm and visceral endoderm [25,26]. In recent years, SMAD4 mutations in patients have been linked to various cardiovascular phenotypes, including coarctation of the aorta, ventricular septal defects, atrial septal defects, and persistent truncus arteriosus [21,22]. Recently, the SMAD4 Tyr95 mutation in a heterozygous form has been linked to patients’ susceptibility to CHD [27], such as ventricular septal defects, bicuspid aortic valve, thoracic aortic aneurism, and patent ductus arteriosus [27].

Although SMAD4 has emerged as a factor in CHD etiology, its precise role(s) in cardiac NC development and aortic arch artery morphogenesis have been disputed. Several groups have investigated the role of SMAD4 in the neural crest during cardiovascular morphogenesis using the Wnt1-Cre1 transgenic mouse strain [28-31]. These studies showed that SMAD4 was necessary for the survival of cardiac NC cells *in vivo*. SMAD4 was also shown to be important for the differentiation of NC cells into vSMCs *in vitro* [31]. However, NC-to-vSMC differentiation *in vivo* was accompanied by NC apoptosis when SMAD4 was ablated using the Wnt1-Cre1 transgenic line, suggesting that NC-to-vSMC differentiation defects *in vivo* may have been secondary to defects in cardiac NC cell survival [31]. In addition, the use of the Wnt1-Cre1 transgenic mouse model may have complicated the interpretation of results. Later studies showed that Wnt1 and Wnt1 signaling are ectopically activated due to the features of the Wnt1-Cre1 transgene [32]. Wnt1, along with BMPs and FGFs, regulates NC development and thus, potential overexpression of Wnt1 could modify phenotypes in NC genetic mutants generated using Wnt1-Cre1 strain [33-35]. Although it is unknown whether cardiac NCs in the Wnt1-Cre1 strain overexpress Wnt1, phenotypic differences between knockout phenotypes using Wnt1-Cre1 and other NC Cre drivers have been reported [36,37]. For example, Olaopa et al showed that embryos in which NC-specific ablation of *Pax3* was mediated using the TFAP2α^{IRESCre} strain exhibited heart defects while embryos with Wnt-1-Cre1-mediated loss of Pax3 did not [37]. Such differences in gene-ablation phenotypes between the Wnt1-Cre1 driver and other NC drivers [35] underscore the importance of investigating the function of SMAD4 using additional NC Cre drivers. Given the critical roles of SMAD4 in various tissues, determining if vSMC defects are a consequence of cardiac NC cell death *in vivo* or if vSMC differentiation can be regulated independently of NC cell death would help clarify the role of SMAD4 in CHD etiologies.

To investigate the role of SMAD4 in the cardiac NC and to distinguish its role in NC differentiation from its role in NC survival, we generated conditional knockout mouse models to ablate SMAD4 in mid-gestation, in a temporal and tissue-specific manner. We examined the expression of αSMA (a smooth muscle marker) as a proxy for vascular smooth muscle differentiation and the extracellular matrix protein, Fibronectin (Fn1), a known regulator of NC-to-vSMC differentiation [36], as a potential mechanism for SMAD4 regulation of NC-to-vSMC differentiation. Our findings suggest that when SMAD4 mRNA is downregulated globally by about 30%, the role of SMAD4 in αSMA expression can be separated from its role in NC survival *in vivo*. Through cell-specific conditional knockout experiments, we showed that SMAD4 is required in the cardiac NC and not in the pharyngeal arch endothelial cells for the development of NC-derived vSMCs. We show that the absence of SMAD4 in the cardiac NC-derived cells at E9.5 leads to their depletion from the pharyngeal arch mesenchyme. Surprisingly and despite the absence of NC-derived cells, PAAs became surrounded with αSMA+ cells derived from an alternative progenitor source and remodeled into the AAAs. This study highlights the requisite role of SMAD4 in the development of cardiac NC and sheds light on the remarkable plasticity of developmental mechanisms and resilience to perturbations during embryogenesis.

2. Results

2.1 SMAD4 regulates smooth muscle differentiation around the 4th pharyngeal arch arteries.

To examine the role of SMAD4 in αSMA expression and Fn1 induction in the PAAs, we assayed the expression patterns of these genes in the pharyngeal arches of E12.5 embryos. In E12.5 embryos, the process of PAA-to-AAA remodeling has begun, evidenced by the regression of the right 6th PAA (compare Fig. 1A with 1B, vessel marked by * in Fig. 1B will regress). At this time of development, *SMAD4 mRNA* is ubiquitously expressed in the pharyngeal mesenchyme (Fig. 1C-C'), *Fn1 mRNA* and protein are enriched around the PAA endothelium (Fig. 1D-E'), and cardiac NCs have differentiated into vSMCs (Fig. 1F-F'). Fn1 is a known mediator of NC-to-vSMC differentiation, and is robustly expressed and localized around αSMA$^+$ NCs, surrounding the PAAs (Fig. 1E-E') [36].

The global loss of SMAD4 during early development results in embryonic lethality between E6.5-E7.5 [25,26]. Mutants with NC-specific loss of SMAD4 mediated by Wnt1-Cre1, which is activated at about E8.0 of development, survive longer and appear grossly normal at E10.5, dying by E12.5 [28-31]. Despite the grossly normal appearance at E10.5, Wnt1-Cre1-mediated deletion of SMAD4 in the NC causes extensive cell death in NC populating pharyngeal arches and in the cardiac NC [30,38]. To avoid early NC death and test the roles of SMAD4 in the differentiation of cardiac NC-derived cells into vSMCs, we first sought to induce the deletion of *SMAD4* after E9.5, the time at which cardiac NCs have already populated the pharyngeal arches. To accomplish this, we first used the R26R$^{CreERT2/CreERT2}$ mouse strain, in which Cre expression can be induced temporally and ubiquitously [39].

The 4th pair of PAAs forms during E10.5 of the mouse development [40,41]. In the morning of E10.5 (30-31 somites), the 4th pharyngeal arches contain a plexus of small vessels; these vessels coalesce into a large 4th PAA by the evening (34-36 somites), with abundant cardiac NC cells surrounding the PAA [40] (this can also be seen in Fig. 8B-green cells).NC-derived cells populate pharyngeal arches by E9.5 [42]. Thus, to ablate SMAD4 before NCs differentiate into vSMCs around the 4th PAA, and to avoid lethality due to the early loss of SMAD4, we injected tamoxifen at 8 am on day E10.5 (Fig. 2A); this is before the large patent lumen of the 4th PAAs forms [15]. *In vitro*, it has been shown that the half-life of SMAD4 is ~9 hours, [43]. Therefore, embryos were analyzed at E12.5 to allow adequate time for Cre-mediated SMAD4 loss; E12.5 embryos were then examined to determine the effect of SMAD4 loss on the expression of αSMA and Fn1.

Cre-mediated deletion of *SMAD4* exon 8 in the SMAD4$^{flox/flox}$ strain results in a SMAD4-null allele (Yang et al., 2002). To select embryos for further molecular and phenotypic analyses, we chose grossly normal embryos, which were the majority of the embryos we isolated (Fig. 3, Table 1), and analyzed SMAD4 ablation by performing Western blots to assay the expression of SMAD4 protein in the posterior region of each embryo (Fig. 3A-C). 47 Smad4$^{flox/flox}$;R26R^{CreERT2} mutant embryos were analyzed for the expression of SMAD4 protein, and 8 grossly-normal looking embryos (Fig. 3B-E, D', E') exhibiting, on average, a ~5-fold decrease in SMAD4 protein expression compared to Cre-negative controls were selected for further analyses. To evaluate the efficiency of Cre-mediated

recombination in the pharyngeal region, we first assayed the expression of the tdTomato Cre reporter, which revealed the presence of efficient recombination at the ROSA reporter locus in the vast majority of pharyngeal cells after tamoxifen injection (Fig. 2A-C), including the pharyngeal arches (Fig. 2D-E). To assay SMAD4 deletion, we measured the expression of *SMAD4 exon 8 mRNA* in the pharyngeal region by *in situ* hybridization. Sections were analyzed by counting the number of *SMAD4 exon 8*-containing mRNA puncta within a defined area. Compared with controls, which contained an average of ~152 SMAD4+ puncta per ROI (2B', F), mutants contained an average of ~97 puncta per ROI (2C', F). Together, these analyses demonstrate that although Cre-mediated recombination was efficient at the reporter locus, the loss of SMAD4 expression was incomplete in the pharyngeal region. Similarly, an incomplete knockdown of *SMAD4 mRNA* was seen in the pharyngeal arches (Fig. 2D-D', E-E').

To assay the consequences of SMAD4 deletion on smooth muscle differentiation and Fn1 expression, we further analyzed the 8 mutant embryos selected above at E12.5. For each mutant-control pair, we measured the mean intensity of αSMA signal and normalized it to DAPI in the same section. At E12.5, αSMA was expressed in multiple cell layers around the pharyngeal arch of the control embryo (Fig. 4A-A'). Out of 8 control-mutant comparisons, 5 had attenuated αSMA expression levels in the mutants (class A), (Fig. 4B-B'), while in 3 control-mutant pairs, αSMA levels in controls and mutants were similar (Class B), (Fig. 4C-C'), quantified in (Fig. 4D-E). Remarkably, this ~62% penetrance in αSMA defects was observed despite a relatively small, ~33%, decrease in total *SMAD4 mRNA* levels in mutant embryos (Fig. 2F). These observations underscore an exquisite dependency of αSMA expression on the levels of SMAD4 in the NC-derived cells.

To determine the mechanisms regulating changes in αSMA levels, we first stained sections from controls and mutants to detect the expression of Fn1, which is required for NC-to-vSMC differentiation, and which is regulated by Tgfβ signaling in some contexts [44,45]. To determine if SMAD4 regulated the expression of Fn1 *in vivo*, we examined the expression of *Fn1 mRNA* and protein at E12.5. However, we did not observe any differences between controls and mutants (Fig. 5A-B'), quantified in (Fig. 5C-F). To test if the reduction in αSMA was a result of changes in NC proliferation or survival, TUNEL assay and pHH3 staining were performed on consecutive sections through the pharyngeal arches (Fig. 5G-I'). The total cell number and cell proliferation were not significantly affected in the mutants (Fig. 5J-K). However, although apoptotic cells were rare, we found a statistically significant increase (from 1.2% to 2.5%) in the fraction of apoptotic cells in mutant embryos (Fig. 5L). Since the majority (>97%) of cells surrounding the 4th PAA were TUNEL-negative, the decreased αSMA expression in ~60% of the mutants cannot be attributed solely to cell death. Taken together, these data suggest that SMAD4 regulates αSMA expression independently of cell survival and Fn1 levels *in vivo*.

2.2 The expression of SMAD4 in the PAA endothelium is not required for Fn1 or αSMA expression.

Although we did not observe a fully penetrant phenotype, our results suggested that SMAD4 was necessary for αSMA expression in NCs within the pharyngeal arches. As we could

not obtain viable embryos with a larger global SMAD4 knockdown, our focus shifted to identifying the specific cell type that required SMAD4 for inducing αSMA expression. In addition, we hypothesized that targeting SMAD4 in a tissue-specific manner, instead of globally, could result in more efficient deletion of SMAD4 without the induction of cell death.

The PAA endothelium is directly adjacent to cardiac NC-derived cells (Fig 1B). A previous conditional knockout study using *Tie2-Cre* revealed that SMAD4 loss in endothelial cells resulted in embryonic lethality by E10.5, with mutant embryos exhibiting cardiovascular defects, aberrant vascular patterning, and abnormal deposition of the ECM protein, laminin, around the dorsal aortae [46]. This study suggested a role for endothelial SMAD4 in cardiovascular morphogenesis; however, embryonic lethality in this strain prevented the analysis of later defects.

To ablate SMAD4 in the endothelium and to avoid embryonic lethality, we used the Cdh5-CreERT2 transgenic mouse strain [47] and injected tamoxifen at E10.5 (Fig. 6A). We then assayed the efficiency of SMAD4 deletion in E12.5 embryos. We found that the ablation of SMAD4 in the endothelium of $Smad4^{flox/flox}$; Cdh5-CreERT2 mutants was highly efficient, with an average of 76% of Cre-reporter+ cells lacking *SMAD4* in five mutants from three independent experiments (Fig. 6B-E").

Quantification of *Fn1* mRNA and protein in E12.5 $Smad4^{flox/flox}$; Cdh5-CreERT2 mutants demonstrated that the loss of *SMAD4* from the endothelium did not affect the levels of *Fn1 mRNA* or protein in NC-derived cells surrounding the 4^{th} PAAs (Fig. 7A-A', B-B,' and C-F). The differentiation of NCs to αSMA^{+} smooth muscle cells was also unaffected (Fig. 7A", B" and G-H). Additionally, the loss of *SMAD4* from the endothelium did not perturb *Fn1 mRNA* expression in the endothelium itself (Fig. 7I-L). These findings indicate that endothelial *SMAD4* is not required for *Fn1* expression in the NC-derived cells surrounding the 4^{th} PAAs, or for their subsequent differentiation into vSMCs. Therefore, these studies suggested that the expression of SMAD4 in cardiac NC-derived cells was required for NC-to-vSMC differentiation.

2.3 The expression of SMAD4 in NC-derived cells is required for their contribution to the pharyngeal mesenchyme and pulmonary valves.

Cardiac NC-derived cells migrate from the dorsal neural tube into the cardiac outflow tract where they contribute to the developing aortic and pulmonary valves and into the pharyngeal region, populating pharyngeal arches [42,48,49]. In the pharyngeal arches, cardiac NC-derived cells comprise multiple cell layers adjacent to the PAA endothelium (Figs. 1B pink, 8B, green). NC-derived cells closest to the pharyngeal arch endothelium differentiate into vSMCs, a process which is indispensable for the remodeling the PAAs into the AAAs [11,16,50].

To investigate the role for SMAD4 in the induction αSMA expression in NCs, we used the Sox10-iCreER^{T2} strain [51] to conditionally ablate SMAD4 in NCs at E9.5, in migrating and post-migratory NCs (Fig. 8A). This time point was chosen because we wanted to a) avoid early NC cell death, as was seen in SMAD4-ablation studies using Wnt1-Cre1 transgenic

strain, in which the onset of Cre recombinase occurs much earlier and encompasses pre-migratory NC as well [28,30,31] and b) at E9.5, cardiac NC-derived cells have already populated the pharyngeal arch mesenchyme, and we wanted sufficient amount of time to pass to ensure SMAD4 deletion before NC progenitors differentiate into vSMCs in the 4th arch, at E10.5. Thus, we injected tamoxifen at E9.5. Upon evaluating SMAD4 knockdown efficiency at E12.5, we made three observations. *First*, when comparing controls (Fig. 8B-B1) with mutants (Fig. 8C-C1), we saw fewer Sox10-lineage cells (green cells in Fig. 8B-B1, C-C1) in the 4th pharyngeal arches (quantified in Fig. 8D). However, despite the reduced number of Sox10-lineage cells around the 4th PAAs in Smad4$^{flox/flox}$;Sox10-iCreER^{T2}mutants, the total number of cells surrounding the arch artery endothelium was not affected (Fig. 8E). *Second*, we observed that the few Sox10-lineage cells remaining in the Smad4$^{flox/flox}$; Sox10-iCreER^{T2} mutants still expressed *SMAD4* mRNA (arrowheads in Fig. 8C-C1, quantified in 8F). *Third*, while controls exhibited a fully Sox10-lineage-derived αSMA layers (Fig. 8B2-B3), in mutants, primarily non-Sox10-lineage compensatory cells contributed to αSMA+ cells around the endothelium (arrows in Fig. 8C2-C3 point to vSMCs of non-neural crest origin, arrowheads point to a few remaining SMAD4+ NC-derived cells).

Since the remaining NCs in the pharyngeal arches of mutants expressed *SMAD4* mRNA, we sought to determine whether SMAD4 was ablated in other NC-derived lineages in Smad4$^{flox/flox}$; Sox10-iCreER^{T2} mutants. Thus, we evaluated *SMAD4* deletion in the dorsal root ganglia (DRGs), which are neural-crest-derived [52]. Our analyses demonstrated that, on average, 97% of NC-derived cells in control DRGs expressed *SMAD4* (Fig. 9A-A", C), while the majority of NC-derived cells in the mutant DRGs lacked *SMAD4* (Fig. 9B-B", C). We also observed that NC-derived neurons in mutants lacked *SMAD4* as well (Fig. 9D-E"). Together, these data show that Sox10-iCreER^{T2} efficiently mediates recombination both at the ROSA reporter and *SMAD4* loci. Therefore, the absence of SMAD4-null NC-derived cells in the 4th pharyngeal arches at E12.5 in the mutants indicates that the expression of SMAD4 in NC-derived cells is required for the contribution of these cells to the pharyngeal arch mesenchyme.

To address whether altered differentiation and/or migration at earlier stages contributed to the paucity of SMAD4-negative NCs in the 4th pharyngeal arches of mutants at E12.5, we injected tamoxifen at E9.5 as above (Fig. 10A) and stained and imaged whole E10.5 control and mutant embryos to detect patterning and differentiation of NC-derived cells. NCs are known to contribute to cranial neurons and glia, and thus, we hypothesized that the loss of SMAD4 could alter the migration or differentiation of the cardiac NCs [53]. Tuj-1 staining revealed normal patterning of NC-derived cranial neurons when comparing control Cre-negative (Fig. 10B-B') and Smad4$^{flox/+}$; Sox10-iCreER^{T2} Cre-positive (Fig. 10C-C'), with Smad4$^{flox/flox}$; Sox10-iCreER^{T2} mutants (Fig. 10D-D'). We next examined NC trans-differentiation to endothelial cells (ECs) (Fig. 11). NC-to-EC differentiation has previously been observed *in vitro* in carotid-body-derived NCs, which expressed EC markers when cultured in defined medium [54]. However, we did not detect any Sox10-lineage cells co-expressing VEGFR2 in the craniofacial (Fig. 11A1, B1), pharyngeal (Fig. 11A2, B2) or trunk regions (Fig. 11A3, B3).

Since NC-derived cells also give rise to the enteric nervous system [52], we examined NC migration toward the gut endoderm at E10.5 by staining for the Cre-reporter. Quantification of Sox10-lineage cells surrounding the endoderm revealed no differences in the number of NC-derived cells among Smad4$^{flox/+}$;Sox10-iCreER^{T2} Cre-positive controls and Smad4$^{flox/flox}$; Sox10-iCreER^{T2} mutant embryos (Fig. 12). Together, these data argue against the notion that SMAD4-null NC cells are reduced in E12.5 pharyngeal arches due to their aberrant migration or due to their differentiation into other lineages.

2.4 SMAD4-null neural crest cells do not persist in the pharyngeal arches after E10.5

Previous studies using the Wnt1-Cre1 strain to ablate SMAD4 in the NC have indicated that SMAD4 is important for the survival of the NCs contributing to the cardiac outflow tract and pharyngeal region [28-31]. Because we saw so few SMAD4-null NCs cells in the pharyngeal arches of E12.5 Smad4$^{flox/flox}$; Sox10-iCreER^{T2} mutant embryos (Fig. 8), we hypothesized that NC survival in the pharyngeal arches was attenuated with Cre-mediated SMAD4 loss at E9.5. To test this, we analyzed the presence of Sox10-lineage cells in the pharyngeal arches 30 hours after tamoxifen administration in Smad4$^{flox/+}$; Sox10-iCreER^{T2} control and Smad4$^{flox/flox}$; Sox10-iCreER^{T2} mutant embryos ranging from 35-37 somites (E10.5). Already at this early time after the injection of tamoxifen, we found fewer Sox10-lineage cells in the 4th pharyngeal arches of Smad4$^{flox/flox}$; Sox10-iCreER^{T2} mutants compared with Smad4$^{flox/+}$; Sox10-iCreER^{T2} controls (Fig. 13). This suggests that Sox10-lineage cells in the pharyngeal arches are highly sensitive to SMAD4 loss. Since NC-derived cells already populate pharyngeal arches at E9.5 (the time of injection [36,42]), these studies indicate that the deletion of SMAD4 causes the loss of pharyngeal NCs, likely due to their apoptosis. Taken together, these data demonstrate the crucial role of SMAD4 in the contribution of NC-derived cells to the pharyngeal arch mesenchyme and show that relative to other NC-derived cell types, the cardiac NC is especially sensitive to the levels of SMAD4.

2.5 Alternative vSMC progenitors rescue the morphogenesis of the aortic arch and its arteries.

Neural crest ablation studies in mice and chick demonstrated the requisite role of the cardiac NC in the morphogenesis of the AAAs, septation of the heart and the outflow tract, and the morphogenesis of aortic and pulmonary valves [37,55,56]. In these studies, cardiac NC was ablated early in its ontogeny, either by surgical means in the chick [55,57] or by the induced expression of cellular toxins such as herpes simplex virus-1 thymidine kinase or diphtheria toxin fragment-A using Wnt1-Cre1 transgenic mice [37,56]. These studies and others demonstrated that the differentiation of NC cells into vSMCs is essential for the persistence of PAAs and their correct remodeling into the AAAs [17,58].

In our studies, tamoxifen was injected at E9.5 to ablate SMAD4 in Sox10-iCreER^{T2} mice, causing a decrease in the number of NC-derived cells in the pharyngeal arches 30 hours later, at E10.75 (Fig. 13) and near-complete depletion of NC-derived cells by E12.5 (Fig. 8). Since we found αSMA+ cells of non-NC origin around the 4th PAAs at E12.5, we asked whether these cells could support the proper AAA development. To address this question, we injected tamoxifen at E9.5, and dissected Smad4$^{flox/+}$; Sox10-iCreER^{T2} control and Smad4$^{flox/flox}$; Sox10-iCreER^{T2} mutant embryos at E16.5. All control

embryos (Cre+ and Cre-negative in this cross, n=8) and 4 out of 4 mutants had typically patterned AAAs (Fig. 14A, B, E). To determine whether smooth muscle cells around arch arteries were derived from the remaining SMAD4+ NC cells or if they came from the alternative progenitor source, we stained coronal paraffin sections of the isolated hearts and AAAs using antibodies to mCherry to detect the expression of the Cre-reporter (cyan) and αSMA to detect vSMCs (orange) (Fig. 14). In control mice, the majority of the aortic arch (AA) vSMCs were derived from the cardiac NC as published before [42] (Fig. 14C-D2). Remarkably, only rare NC-derived cells could be seen in the smooth muscle coat of the ascending aorta and the AA in Smad4$^{flox/flox}$; Sox10-iCreER^{T2} mutants (Fig. 14F-G2). Similarly, while pulmonary valves had multiple NC-derived cells in Smad4$^{flox/+}$; Sox10-iCreER^{T2} controls (Fig. 14C), no NC-derived cells were present in the valves of Smad4$^{flox/flox}$; Sox10-iCreER^{T2} mutants (Fig. 14F, arrowheads). We did not observe cardiac septation defects in the mutant hearts either. These results indicate that when NC-derived cells are depleted later in development (but before PAAs are fully formed), alternative vSMC progenitors in the arches and the heart can replace NC-derived cells and lead to the proper septation, valve development and remodeling of the AAAs. Although we don't know what the compensating cells are, mesodermal cells from the second heart field (SHF) have the capacity to give rise to vSMCs, and typically do give rise to vSMCs at the base of the ascending Aorta (aAo) and Pulmonary Trunk (PT) [59,60]. SHF-derived mesodermal cells are present in the pharyngeal arch mesenchyme and the cardiac outflow tract at E9.5 [61,62], the time when tamoxifen is injected into Sox10-iCreER^{T2} animals in our experiments. We hypothesize that SHF-derived mesoderm compensates for the lack of NC-derived cells and rescues AAA morphogenesis in Smad4$^{flox/flox}$; Sox10-iCreER^{T2} mutants.

3. Discussion

SMAD4 is a central signaling mediator in the canonical TGF β and BMP pathways. While SMAD4 has well-documented tumor suppressor activity [23,63], recently, missense mutations in SMAD4 have been linked to a genetic predisposition for CHD [21,24,27]. Because of the evolving role of SMAD4 in CHD phenotypes, we sought to further elucidate its contribution to the morphogenesis of the 4th PAAs, whose remodeling defects, such as the interrupted aortic arch are life-threatening if left untreated [8]. To do this, we probed the role of SMAD4 in vSMC differentiation of the cardiac NC, a process that is indispensable for AAA morphogenesis.

SMAD4 regulates αSMA expression in the 4th pharyngeal arches.

NC differentiation to vSMCs is critical in the proper arch artery morphogenesis [11,16,17,55,64]. Failure of NCs to differentiate into vSMCs can result in premature PAA regression. Various factors have been implicated in vSMC differentiation of the neural crest *in vivo*, including *ALK2*, NOTCH signaling, *Fn1*, and the SMAD2/MRTFβ signaling axis [36,65-67]. When using the R26R^{CreERT2} strain [39] to achieve a global loss of SMAD4, we observed small (~1.5-fold on average) and graded levels of SMAD4 deletion. The appreciable SMAD4 levels which remain in the tissue may in part be explained by the inefficiency or low expression levels of the Cre recombinase. Unlike the transgenic Cdh5-CreERT2 [47] strain used in this study, which encodes multiple copies of the Cre gene, R26R^{CreERT2} strain encodes a single copy

of the Cre recombinase gene knocked into the ROSA26 locus [39]. In addition, the inefficient deletion of SMAD4 may be due to low levels of Cre-ERT2 protein in R26R^{CreERT2} strain, which has to act on 3 pairs of floxed loci upon tamoxifen induction: 2 pairs at each of the SMAD4 exon 8 loci, and 1 pair at the ROSA26 tdTomato reporter locus. Alternatively, only cells with incomplete deletion in the *SMAD4* locus survive and proliferate, giving rise to multiple embryonic lineages, including the cardiac NC. Although, Sox10-iCreER^{T2} is also a knock-in strain [51], the efficient deletion of SMAD4 in multiple NC-derived lineages in this strain could be due to a higher level of Cre expression than in R26R^{CreERT2} strain due to the differences in promoter/enhancer activities. Alternatively, the expression of SMAD4 in some NC-derived lineages (neurons and glia) is not required for their development. Despite the small changes in *SMAD4* mRNA levels when using R26R^{CreERT2} strain, αSMA expression was attenuated in 62% of mutants. Defects in vSMC differentiation were unlikely caused by apoptosis, since the percentage of apoptotic cells, although increased in the mutants, was overall very small (<3%). These studies suggest that the role of SMAD4 in the differentiation of NC cells to smooth muscle cells is uncoupled from its role in cell survival, consistent with findings *in vitro* [31].

Potential role of SMAD4 in regulating Fn1 expression in the 4th pharyngeal arches.

To explore potential mechanisms underlying how SMAD4 regulates NC-to-vSMC differentiation, we investigated SMAD4 regulation of the extracellular matrix protein, Fn1. Our lab previously found that Fn1 has a dynamic expression pattern in NCs and that it is critical for NC-to-vSMC differentiation and PAA-to-AAA remodeling [36]. There are a number of studies that indicate that TGFβ stimulation induces Fn1 synthesis both *in vitro* and *in vivo* in fibrotic tissue, where TGFβ ligands are often seen upregulated as part of the inflammatory response (Hocevar et al., 1999; Ignotzs & Massague, 1986; Walton et al., 2017). We found that the expression of *Fn1* mRNA and protein were unaffected by the small decrease in SMAD4 levels. Thus, in contrast to αSMA, Fn1 expression was less sensitive to changes in SMAD4 levels. Additionally, these data show that SMAD4 regulates αSMA levels independently of Fn1.

Endothelial SMAD4 is not required for αSMA or Fn1 expression.

It has been previously shown that Tie2-Cre mediated loss of SMAD4 from the endothelium results in embryonic lethality by E10.5, with embryos exhibiting defects in the heart and vessel formation [46]. To ablate SMAD4 in a narrow window of time and avoid the lethality associated with the early ablation of SMAD4, we utilized the Cdh5-iCreERT2 strain to delete SMAD4 from the endothelium at E10.5. The Cdh5-iCreERT2 strain allowed for efficient downregulation of SMAD4 expression in the endothelium. Despite the near-complete loss of *SMAD4* in the PAA precursors, we did not observe anomalies in pharyngeal arch artery formation. *Fn1* mRNA levels produced by endothelial cells were unchanged, and *Fn1* mRNA and protein expression in the surrounding NC cells were also unaffected. Similarly, there were no changes in αSMA expression in the surrounding NC-derived cells. Altogether, our data suggest a) endothelial SMAD4 does not regulate Fn1 expression and b) that fluctuations in αSMA protein levels in NC-derived cells surrounding the PAA endothelium in Smad4$^{flox/flox}$; R26R^{CreERT2} mutants are attributable to SMAD4 expression changes in the NC.

The expression of SMAD4 in the NC is required for the contribution of NC-derived cells to the vascular smooth muscle cell coat of the pharyngeal arch arteries.

Using the Sox10-iCreER^{T2} inducible strain to conditionally delete SMAD4 from the NC-derived cells following their arrival into the pharyngeal arches, we found a significantly reduced number of Sox10-lineage cells surrounding the 4th pharyngeal arches in mutants compared to controls. However, despite the successful ablation of *SMAD4* in NC-derived tissues such as the dorsal root ganglia, the few Sox10-lineage (Cre+) cells remaining at E12.5 in the 4th PAs expressed *SMAD4* mRNA. The presence of a small population of reporter+; SMAD4+ NCs that remained in pharyngeal arches of Smad4$^{flox/flox}$; Sox10-iCreER^{T2} mutants at E12.5 could be due to the survival of NC-derived cells that retained SMAD4. These NCs may not have undergone Cre-mediated recombination at the loxP sites in the SMAD4 locus upon tamoxifen injection, due to the fact that Cre-mediated recombination is never 100% efficient [51]. The lack of SMAD4-negative NCs around the 4th PAAs indicates the indispensable role of SMAD4 in the contribution of NC-derived cells to the pharyngeal mesenchyme.

Since SMAD4-null NCs were not observed in the pharyngeal arches at E12.5, we sought to identify their fate. Cardiac NCs, which contribute to the developing pharyngeal arches and the cardiac outflow tract, are part of a larger population of cranial NCs [19,48]. In addition to cranial placodes, cranial NCs contribute to sensory neurons as well as the sensory ganglia in cranial nerves I, II, V, VII, VIII, IX, X, and XI of the peripheral nervous system [68,69]. In addition, it has been shown that NC-derived cells can differentiate into endothelial cells when cultured in defined media [54]. Overall, our experiments analyzing the expression of Tuj-1, VEGFR2, and the Sox10-lineage reporter indicated that the loss of SMAD4 in the NC lineage did not expand the fate potential of NCs or cause aberrant migration of these cells.

NC-derived cells are observed in the pharyngeal arches at E9.5, the time of tamoxifen injection [14,36]. Quantification of NC-derived cells at E10.5, 30 hours after the injection of tamoxifen, showed a statistically significant decrease in the number of Sox10-lineage cells in the pharyngeal arches of mutants compared with controls. This finding demonstrates a stringent requirement for SMAD4 for the contribution of NCs to the pharyngeal arch mesenchyme.

Despite the reduced number of Sox10 lineage cells, the total number of cells in the 4th pharyngeal arches were equivalent between controls and mutants. Even though the number of NC-derived cells were dramatically reduced in the mutants, the αSMA expression was unaltered around the 4th PAAs. Furthermore, the presence of αSMA+ cells from the alternative source allowed for the persistence and proper remodeling of PAAs to AAAs. The ability to examine the presence of Sox10-lineage+ cells in these embryos allowed us to conclude that αSMA+ cells surrounding the PAA and AAA endothelium were mainly formed by SMAD4+ cells of non-NC origin.

While we have not investigated the source of these compensatory vSMCs, one possibility is that they are second-heart field derived since the SHF-derived mesoderm is present in the pharyngeal arches and the heart [61,62]. In addition, it has been previously shown that SHF-derived cells are competent to contribute, in part, to smooth muscle cells in other

vessels, including the proximal ascending aorta and pulmonary trunk [59,70]; Additional studies are needed to investigate this hypothesis, however. One future direction for this work would be to examine the phenotypic consequences of vSMCs formed from non-NC-derived cells compared to NC-derived ones. While the smooth muscle layer is formed, the function of mesodermal-derived vSMCs may differ from NC-derived vSMCs. It has been gleaned from *in vitro* studies that vSMCs of different origins have different phenotypic and genetic features, including cell shape, regulatory genetic networks, as well as response to growth factors and inhibitors [71-74]. Furthermore, these differences may underlie vascular disease states, including aortic aneurysms and vascular calcification [75-77].

Our studies are valuable because they confirm the indelible role of SMAD4 in cardiac NC cell survival using a different set of reagents. In addition, we discovered that cells of non-NC origin differentiate into smooth muscle cells to compensate for the reduced numbers of NC-derived cells in the arches. Altogether, our studies highlight the incredible plasticity of developmental mechanisms to ensure arch artery morphogenesis in the face of severe perturbations.

4. Experimental Procedures

4.1 Mouse strains and Generation of Mutants

All animals were maintained in accordance with the regulations of Rutgers Animal Care and the Rutgers International Animal Care and Use Committee (IACUC). The following mouse strains were used in this study (see Table 2): Smad4$^{tm2.1cxd}$/J [78]; JAX Stock no. 017462, here referred to as **Smad4$^{flox/flox}$**, B6.129-Gt(ROSA)26Sortm1(cre/ERT2)Tyj/J [39]; JAX Stock no. 008463, here referred to as **R26R$^{CreERT2/CreERT2}$**, CBA;B6-Tg(Sox10-icre/ERT2)388Wdr/J [51]; JAX Stock no. 027651, here referred to as **Sox10-iCreER^{T2}**, and B6.Cg-Gt(ROSA)26Sortm9(CAG-tdTomato)Hze/J [79]; JAX Stock no. 007909, here referred to as **R26R$^{Td/Td}$** mice.

C57BL/6-Tg(Cdh5-Cre/ERT2)1Rha mice [47] were a gift from Dr. Ralf Adams, Max Planck Institute for Molecular Biomedicine, Münster, Germany.

Smad4$^{flox/flox}$;R26R$^{Td/Td}$ females were generated by crossing Smad4$^{flox/flox}$ and R26R$^{Td/Td}$ mice. Smad4$^{flox/+}$;R26R$^{CreERT2/TdTom}$ males were generated by crossing Smad4$^{flox/flox}$;R26R$^{Td/Td}$ females to R26R$^{CreERT2/CreERT2}$ males. Smad4$^{flox/+}$;Sox10-iCreER^{T2} males were generated by crossing Smad4$^{flox/flox}$;R26R$^{Td/Td}$ females to Sox10-iCreER^{T2} males. To generate Smad4$^{flox/+}$;Cdh5-CreERT2 males, Smad4$^{flox/flox}$;R26R$^{Td/Td}$ females were crossed with Cdh5-CreERT2 males.

To ablate SMAD4 globally, Smad4$^{flox/flox}$; R26R$^{Td/Td}$ females were crossed with Smad4$^{flox/+}$;R26R$^{CreERT2/Td}$ males. To ablate SMAD4 in the endothelium, Smad4$^{flox/flox}$; R26R$^{Td/Td}$ females were crossed with Smad4$^{flox/+}$;Cdh5-CreERT2 males, and to ablate SMAD4 in the neural crest, Smad4$^{flox/flox}$; R26R$^{Td/Td}$ females were crossed with Smad4$^{flox/+}$;Sox10-iCreERT2 males. Pregnant mothers were injected intraperitoneally with Tamoxifen to induce Cre-Lox recombination, as described below.

4.2 Tamoxifen Injections

Tamoxifen (Sigma Aldrich, T5648) was dissolved in sesame oil (Sigma Aldrich, S3547) at a concentration of 10 mg/ml by vortexing for 2 hours at room temperature before intraperitoneal administration into pregnant mothers. In studies with $R26R^{CreERT2/CreERT2}$ mice, 3 mg of tamoxifen dissolved in 300 µl of corn oil (MP Biomedicals, 901414) was injected i.p. into the pregnant dams at 8 am of E10.5. For studies involving Cdh5-CreERT2 strain, pregnant dams were injected with 1.5 mg of tamoxifen at 8 am of E10.5. For and Sox10-iCreER^{T2} strain, 1.5 mg of tamoxifen was injected at 10 am of E9.5. The timelines of injection and embryo collection are outlined in each figure.

4.3 Genotyping

To obtain embryonic DNA, murine embryonic yolk sacs were incubated overnight in lysis buffer (1M Tris pH 8.5; 0.5M EDTA; 5M NaCl; 20% SDS) containing 0.02 mg/ml proteinase K (ThermoFisher, EO0492) at 58° C in a ThermoMixer F1.5 (Eppendorf). To precipitate DNA, 100% isopropanol was added to each sample, and precipitated DNA was dissolved in dH_2O overnight at 37° C in a ThermoMixer. Genotyping was done by PCR. For genotyping the SMAD4 floxed allele, primers listed in [28] were used, resulting in a 282 bp PCR product for the wild-type allele and a 330 bp PCR product for the floxed allele. For detecting the $R26R^{CreERT2}$ allele, Cre-specific primers 5'- CTA GAG CCT GTT TTG CAC GTT C-3' and 5'-GTT CGC AAG AAC CTG ATG GAC-3' were used, resulting in a 320 bp PCR product. For detecting the Sox10-iCreER^{T2} allele, the following primers to the *improved* Cre (iCre) were used: 5'-CTG TGG ATG CCA CCT CTG ATG-3' and 5'-GCC AGG TTC CTG ATG TCC TG-3' generating a 442 bp PCR product.

4.4 Tissue-processing and preparation of formalin-fixed paraffin-embedded (FFPE) sections

Embryos were dissected in cold 1X Phosphate-buffered saline (PBS), prepared from a 10% stock solution (ThermoFisher, J75889-K2), and fixed in 10% Neutral-buffered Formalin (VWR, 10790-714) for 16 hours at room temperature. Embryos were then washed in 1X PBS and dehydrated via a series of graded ethanol (EtOH) solutions made in water. For E12.5 embryos and E16.5 hearts, sampes were incubated for 1 hour at room temperature in 70%, 80%, and then 90% EtOH with agitation. Embryos were then incubated twice in 100% EtOH, for 1 hour each, at room temperature. Embryos were then incubated in Xylene twice for 30 min each, and in paraffin 70° C, twice for 30 min each. For E10.5, embryos were incubated in 70% EtOH for 3 min, and 80% EtOH for 3 min. Then, embryos were incubated in 95% EtOH twice, for 5 min each, then once for 10 min, and finally in 100% EtOH three times, for 10 min each. Embryos were then incubated in Xylene twice for 20 min each, and in paraffin at 70° C, twice for 20 min each. Embryos were then embedded into paraffin, and 5 µm sections were collected using Leica Biosystems Rotary Microtome Manual HistoCore BIOCUT.

4.5 TUNEL and pHH3 Analyses

For antigen retrieval, FFPE slides were first baked in a 60°C dry oven for 20 minutes. Slides were then rehydrated with Xylene and decreasing grades of ethanol (100%-70%).

Slides were then boiled for 10 minutes in 10mM Sodium Citrate solution, pH 6.0. Following antigen retrieval, Terminal deoxynucleotidyl transferase-mediated dUTP nick-end labeling (TUNEL) was performed, according to manufacturer's protocols (Sigma, 11684795910, Table 3, protocol **#1**). For staining, slides were first permeabilized in 1X Phosphate-buffered saline with 0.05% Tween-20 (Sigma, P7949), PBST, 3x, for 5 minutes each, and then blocked with blocking buffer (5% normal donkey serum in 0.05% PBST). Slides were then incubated in primary antibody, Rabbit anti- Phospho-Histone H3 primary antibody (1:100, Cell Signaling Technology, 9701), overnight at 4°C. After washing, slides were incubated in donkey anti-Rabbit 555 secondary (1:300, ThermoFisher, A-31572) for 1 hour. DAPI (1:1000 dilution of 5mg/mL stock made in dH2O, ThermoFisher, D3571) was included in secondary antibody solution. Following immunohistochemistry, slides were washed and mounted with ProLong gold antifade solution (ThermoFisher, P36930).

4.6 Multiplex Fluorescence in situ hybridization

For detection of *Fn1* mRNA, tissue sections were first embedded into paraffin and cut into 5 μm sections, as described above. *In situ* hybridization was performed to detect *Fn1* mRNA using a probe (ACD, 408181) according to instructions in the Multiplex Fluorescent Kit v2 (323100) from ACD (Table 3, protocol **#2**). Bound probes were detected using TSA Plus fluorophores Cyanine 5 (Akoya Bioscience, NEL745001KT) and Cyanine 3 (Akoya Bioscience, NEL744001KT) according to manufacturer protocols; see Table 3, protocol **#2**.

Following transcript detection, immunofluorescence was performed according to the *ACD Inc.* protocol listed below (Table 3, protocol **#3**). The following antibodies were used: Rabbit anti-mCherry (1:1000, Abcam, ab167453), recombinant rabbit anti-Fibronectin (1:1000, Abcam, ab19056), and mouse anti-αSMA (1:500, Sigma Aldrich, A5228). Primary antibodies were detected with secondary antibodies from Invitrogen (1:300): donkey anti-rabbit conjugated to Alexa-488 (A21206) and donkey anti-mouse conjugated to Alexa-555 (A31570). Secondary antibody solutions also included DAPI (1:1000 dilution of 5mg/mL stock made in dH_2O, ThermoFisher, D3571). Following immunohistochemistry, samples were mounted with ProLong gold antifade solution (ThermoFisher, P36930).

4.7 Base-scope in situ hybridization and Immunofluorescence

In the $Smad4^{flox/flox}$ strain, Smad4 exon 8 is flanked by two loxP sites. Cre-mediated recombination of Smad4 exon 8 results in a null allele[78]. Therefore, using formalin-fixed paraffin embedded sections (prepared as above) we assayed the presence of the SMAD4 exon 8 sequence (51 bps) and performed downstream immunofluorescence for the Cre reporter according to the *Basescope RED* + IHC protocol, see Table 3, protocol **#4** (*ACD Inc.*, 323900). Samples were mounted with ProLong gold antifade solution.

4.8 Whole-mount immunofluorescence

Whole-embryo immunofluorescence of E10.5 embryos was performed as previously described in [78]. The primary antibodies used were: Rabbit anti-mCherry (1:1000, Abcam, ab167453), Mouse anti-Tuj1 (1:150, Covance, MMS-435P), and Goat anti-VEGFR2 (1:200, R&D Systems Inc., AF644). Primary antibodies were detected with secondary antibodies from Invitrogen (1:300): donkey anti-rabbit conjugated to Alexa 555 (A31572), donkey anti-

mouse conjugated to Alexa-647 (A31571), and donkey anti-goat conjugated to Alexa-488 (A11055). Secondary antibody solutions also included DAPI, as above.

4.9 Immunoblotting

For SMAD4 protein quantification, the posterior region of the tail of each E12.5 embryo was used. Tissue specimens were resuspended in 500μl of lysis buffer (1M Tris-HCl, 0.2% SDS, 5 mM EDTA, 1X protease inhibitor) and dissociated using a 27-gauge syringe. After tissue dissociation, samples were boiled for 10 minutes at 95°C in 140 mM β-mercaptoethanol and 1x NuPage loading buffer (ThermoFisher, NP0007). Each sample was then run on a 4-12% Novex gel (ThermoFisher, XP04120BOX) in 1X Tris-Glycine SDS running buffer (ThermoFisher, LC2675) for 1.25 hours at 130V. Proteins were blotted onto a nitrocellulose membrane (BIO-RAD, 1620112) for 2 hours at 60V on ice. The membrane was then washed in 1X Phosphate-buffered saline with 0.01% Tween-20 (PBST) 3x, for 5 minutes each and then blocked in Intercept TBS blocking buffer (LI-COR, 927-66003) for 1 hour. The membrane was then incubated in rabbit anti-Smad4 primary antibody (1:5000, Abcam, ab 40759), overnight on an orbital shaker at 4°C. After washing (as above) the following day, the membrane was incubated in mouse anti-β actin (1:10,000, Cell Signaling Technology, 3700S) for 1 hour on a room temperature orbital shaker. The membrane was then washed again and then incubated in IRDye 680RD Donkey anti-Rabbit IgG (LI-COR, 926-68073), and IRDye 800CW Donkey anti-Mouse IgG Secondary Antibody (LI-COR, 926-32212), each diluted at 1:10,000, for 1 hour on a room temperature orbital shaker. All primary and secondary antibodies were diluted in intercept diluent (LI-COR, 927-66003). Membranes were developed with LI-COR Odyssey digital imaging system. Quantification of signal intensity was performed using ImageJ software (National Institutes of Health).

4.10 Image Visualization and Analysis

Confocal images were acquired with the Nikon A1 confocal microscope using a 20X CFI Apo LWD Lamda S water immersion objective (MRD77200). Images of sections and whole embryos were analyzed with ImageJ software (National Institutes of Health) and Imaris Viewer, version 9.9.1 (Oxford Instruments), respectively. To assay the expression of Smad4 in the pharyngeal region of $R26R^{CreERT2}$ samples, a defined region of interest (ROI) was drawn within the pharyngeal region, and the number of Smad4 puncta per ROI was counted. Identically sized ROIs were used for analyses of control and mutant samples. To validate Smad4 loss in the endothelium and neural crest, the percentage of Smad4+ nuclei was quantified in Cre-reporter+ cells. To measure *Fn1 mRNA*, Fn1 protein, and αSMA expression levels around the pharyngeal arches, mean fluorescence intensity was measured as shown in the figures and the signal intensity was normalized to DAPI for the corresponding ROI.

Acknowledgments:

We would like to thank all members of the Astrof lab for their careful editing of this manuscript: Michael Warkala, Dr. Cecilia Arriagada, and Dr. Gideon Obeng. We would also like to thank Drs. Melissa Rogers, Steven Levison, and Theresa Wood of the Rutgers Biomedical Sciences Graduate Program for their feedback on experiments. We would also like to thank the faculty and staff of the Rutgers University Animal Care Facilities for assistance with animal husbandry. BEA would also like to thank Sam Russo for his help with tissue histology, Michael Warkala and

AnnJosette Ramirez for their help with embryo handling, and Shabazz Hall for her support and encouragement in the preparation of this manuscript.

Funding:

This work was supported by funding from the National Heart, Lung, and Blood Institute of the National Institutes of Health: R01 HL103920, R01 HL134935, and R01 HL158049 to S.A., a pre-doctoral fellowship from the National Heart, Lung, and Blood Institute F31HL151046 to B.E.A., and a postdoctoral fellowship from the American Heart Association to HZ, 23POST1022380.

References

1. Bulatovic I, Månsson-Broberg A, Sylvén C, Grinnemo KH. Human fetal cardiac progenitors: The role of stem cells and progenitors in the fetal and adult heart. Best Practice and Research: Clinical Obstetrics and Gynaecology. 2016;31:58–68. https://doi.org10.1016/j.bpobgyn.2015.08.008. [PubMed: 26421632]
2. Buckingham M, Meilhac S, Zaffran S. Building the mammalian heart from two sources of myocardial cells. Nature Reviews Genetics. 2005;6(11):826–835. https://doi.org10.1038/nrg1710.
3. Bouma BJ, Mulder BJM. Changing Landscape of Congenital Heart Disease. Circulation Research. 2017;120(6):908–922. https://doi.org10.1161/CIRCRESAHA.116.309302. [PubMed: 28302739]
4. Oster ME, Lee KA, Honein MA, Riehle-Colarusso T, Shin M, Correa A. Temporal trends in survival among infants with critical congenital heart defects. Pediatrics. 2013;131(5). https://doi.org10.1542/peds.2012-3435.
5. Dolk H, Loane M, Garne E. Congenital heart defects in Europe: Prevalence and perinatal mortality, 2000 to 2005. Circulation. 2011;123(8):841–849. https://doi.org10.1161/CIRCULATIONAHA.110.958405. [PubMed: 21321151]
6. Mahle WT, Newburger JW, Matherne GP, et al. Role of pulse oximetry in examining newborns for congenital heart disease: A scientific statement from the AHA and AAP. Pediatrics. 2009;124(2):823–836. https://doi.org10.1542/peds.2009-1397. [PubMed: 19581259]
7. Wu W, He J, Shao X. Incidence and mortality trend of congenital heart disease at the global, regional, and national level, 1990-2017. Medicine (United States). 2020;99(23). https://doi.org10.1097/MD.0000000000020593.
8. Jackson CE, Weiss L, Reynolds WA, Forman TF, Peterson JA. Interrupted aortic arch in infancy. Journal of Pediatrics. 1976;88(6):963–968. https://doi.org10.1016/S0022-3476(76)81050-5. [PubMed: 1271196]
9. Varghese R, Saheed SB, Omoregbee B, Ninan B, Pavithran S, Kothandam S. Surgical Repair of Interrupted Aortic Arch and Interrupted Pulmonary Artery. Annals of Thoracic Surgery. 2015;100(6):e139–e140. https://doi.org10.1016/j.athoracsur.2015.07.064. [PubMed: 26652572]
10. Graham A, Hikspoors J, Anderson RH, Lamers WH, Bamforth SD. A revised terminology for the pharyngeal arches and the arch arteries. J Anat. May 29 2023. https://doi.org10.1111/joa.13890.
11. Kirby ML, Waldo KL. Neural crest and cardiovascular patterning. Circulation Research. 1995;77(2):211–215. https://doi.org10.1161/01.RES.77.2.211. [PubMed: 7614707]
12. Anderson RH, Bamforth SD. Morphogenesis of the Mammalian Aortic Arch Arteries. Frontiers in Cell and Developmental Biology. 2022;10(May):1–14. https://doi.org10.3389/fcell.2022.892900.
13. Waldo K, Miyagawa-Tomita S, Kumiski D, Kirby ML. Cardiac neural crest cells provide new insight into septation of the cardiac outflow tract: Aortic sac to ventricular septal closure. Developmental Biology. 1998;196(2):129–144. https://doi.org10.1006/dbio.1998.8860. [PubMed: 9576827]
14. Jiang X, Rowitch DH, Soriano P, McMahon AP, Sucov HM. Fate of the mammalian cardiac neural crest. Development. 2000;127(8):1607–1616. [PubMed: 10725237]
15. Wang X, Chen D, Chen K, Jubran A, Ramirez AJ, Astrof S. Endothelium in the pharyngeal arches 3, 4 and 6 is derived from the second heart field. Developmental Biology. 2017;421(2):102–111. https://doi.org10.1016/j.ydbio.2016.12.010.
16. Bergwerff M, Verberne ME, DeRuiter MC, Poelmann RE, Gittenberger-de Groot AC. Neural crest cell contribution to the developing circulatory system implications for vascular morphology?

Circulation Research. 1998;82(2):221–231. https://doi.org10.1161/01.RES.82.2.221. [PubMed: 9468193]

17. Stoller JZ, Epstein JA. Cardiac neural crest. Seminars in cell & developmental biology. 2005;16(6):704–715. https://doi.org10.1016/j.semcdb.2005.06.004. [PubMed: 16054405]
18. Plein A, Fantin A, Ruhrberg C. Neural crest cells in cardiovascular development. 1 ed.: Elsevier Inc.; 2015:183–200.
19. Keyte A, Hutson MR. The neural crest in cardiac congenital anomalies. Differentiation. 2012;84(1):25–40. https://doi.org10.1016/j.diff.2012.04.005. [PubMed: 22595346]
20. Pierpont ME, Brueckner M, Chung WK, et al. Genetic Basis for Congenital Heart Disease: Revisited: A Scientific Statement from the American Heart Association. 2018:e653–e711.
21. Caputo V, Cianetti L, Niceta M, et al. A restricted spectrum of mutations in the SMAD4 tumor-suppressor gene underlies myhre syndrome. American Journal of Human Genetics. 2012;90(1):161–169. https://doi.org10.1016/j.ajhg.2011.12.011. [PubMed: 22243968]
22. Le Goff C, Mahaut C, Abhyankar A, et al. Mutations at a single codon in Mad homology 2 domain of SMAD4 cause Myhre syndrome. Nature Genetics. 2012;44(1):85–88. https://doi.org10.1038/ng.1016.
23. Zhao M, Mishra L, Deng CX. The role of TGF-β/SMAD4 signaling in cancer. International Journal of Biological Sciences. 2018;14(2):111–123. https://doi.org10.7150/ijbs.23230. [PubMed: 29483830]
24. Lin LH, Chang KW, Cheng HW, Liu CJ. SMAD4 Somatic Mutations in Head and Neck Carcinoma Are Associated With Tumor Progression. Frontiers in Oncology. 2019;9(December):1–12. https://doi.org10.3389/fonc.2019.01379. [PubMed: 30761267]
25. Sirard C, de la Pompa JL, Elia A, et al. The tumor suppressor gene Smad4/Dpc4 is required for gastrulation and later for anterior development of the mouse embryo. Genes & Development. 1998;12(1):107–119. https://doi.org10.1101/gad.12.1.107. [PubMed: 9420335]
26. Yang X, Li C, Xu X, Deng C. The tumor suppressor SMAD4/DPC4 is essential for epiblast proliferation and mesoderm induction in mice. Proceedings of the National Academy of Sciences. 1998;95(7):3667–3672. https://doi.org10.1073/pnas.95.7.3667.
27. Wang Y, Xu YJ, Yang CX, et al. SMAD4 loss-of-function mutation predisposes to congenital heart disease. European Journal of Medical Genetics. 2023;66(1):104677–104677. https://doi.org10.1016/j.ejmg.2022.104677. [PubMed: 36496093]
28. Ko SO, Chung IH, Xu X, et al. Smad4 is required to regulate the fate of cranial neural crest cells. Developmental Biology. 2007. https://doi.org10.1016/j.ydbio.2007.09.050.
29. Jia Q, McDill BW, Li SZ, Deng C, Chang CP, Chen F. Smad signaling in the neural crest regulates cardiac outflow tract remodeling through cell autonomous and non-cell autonomous effects. Developmental Biology. 2007;311(1):172–184. https://doi.org10.1016/j.ydbio.2007.08.044. [PubMed: 17916348]
30. Nie X, Deng Cx, Wang Q, Jiao K. Disruption of Smad4 in neural crest cells leads to mid-gestation death with pharyngeal arch, craniofacial and cardiac defects. Developmental Biology. 2008;316(2):417–430. https://doi.org10.1016/j.ydbio.2008.02.006. [PubMed: 18334251]
31. Buchmann-Moller S, Miescher I, John N, Krishnan J, Deng CX, Sommer L. Multiple lineage-specific roles of Smad4 during neural crest development. Developmental Biology. 2009. https://doi.org10.1016/j.ydbio.2009.04.001.
32. Lewis AE, Vasudevan HN, O'Neill AK, Soriano P, Bush JO. The widely used Wnt1-Cre transgene causes developmental phenotypes by ectopic activation of Wnt signaling. Developmental Biology. 2013;379(2):229–234. https://doi.org10.1016/j.ydbio.2013.04.026. [PubMed: 23648512]
33. Litsiou A, Hanson S, Streit A. A balance of FGF, BMP and WNT signaling positions the future placode territory in the head. Development. 2005;132(18):4051–4062. https://doi.org10.1242/dev.01964. [PubMed: 16093325]
34. Debbache J, Parfejevs V, Sommer L. Cre-driver lines used for genetic fate mapping of neural crest cells in the mouse: An overview. Genesis. 2018;56(6-7). https://doi.org10.1002/dvg.23105.
35. Barriga EH, Trainor PA, Bronner M, Mayor R. Animal models for studying neural crest development: Is the mouse different? Development (Cambridge). 2015;142(9):1555–1560. https://doi.org10.1242/dev.121590.

36. Wang X, Astrof S. Neural crest cell-autonomous roles of fibronectin in cardiovascular development. Development (Cambridge). 2016;143(1):88–100. https://doi.org10.1242/dev.125286.
37. Olaopa M, Zhou HM, Snider P, et al. Pax3 is essential for normal cardiac neural crest morphogenesis but is not required during migration nor outflow tract septation. Developmental Biology. 2011;356(2):308–322. https://doi.org10.1016/j.ydbio.2011.05.583. [PubMed: 21600894]
38. Jia Q, McDill BW, Li SZ, Deng C, Chang CP, Chen F. Smad signaling in the neural crest regulates cardiac outflow tract remodeling through cell autonomous and non-cell autonomous effects. Developmental Biology. 2007. https://doi.org10.1016/j.ydbio.2007.08.044.
39. Ventura A, Kirsch DG, McLaughlin ME, et al. Restoration of p53 function leads to tumour regression in vivo. Nature. 2007;445(7128):661–665. https://doi.org10.1038/nature05541. [PubMed: 17251932]
40. Wang X, Chen D, Chen K, Jubran A, Ramirez A, Astrof S. Endothelium in the pharyngeal arches 3, 4 and 6 is derived from the second heart field. Dev Biol. Jan 15 2017;421(2):108–117. https://doi.org10.1016/j.ydbio.2016.12.010. [PubMed: 27955943]
41. Li P, Pashmforoush M, Sucov HM. Mesodermal retinoic acid signaling regulates endothelial cell coalescence in caudal pharyngeal arch artery vasculogenesis. Dev Biol. Jan 1 2012;361(1):116–24. https://doi.org10.1016/j.ydbio.2011.10.018. [PubMed: 22040871]
42. Jiang X, Rowitch DH, Soriano P, McMahon AP, Sucov HM. Jiang et al. - 2000 - Fate of the mammalian cardiac neural crest. 2000;1616:1607–1616.
43. Lin X, Liang M, Liang YY, Brunicardi FC, Feng XH. SUMO-1/Ubc9 promotes nuclear accumulation and metabolic stability of tumor suppressor Smad4. Journal of Biological Chemistry. 2003;278(33):31043–31048. https://doi.org10.1074/jbc.C300112200. [PubMed: 12813045]
44. Hocevar BA, Brown TL, Howe PH. TGF-β induces fibronectin synthesis through a c-Jun pathway. EMBO journal. 1999;18(5):1345–1356. [PubMed: 10064600]
45. Ignotzs RA, Massague J. THE JOURNAL Transforming Growth Factor-@ Stimulates the Expression of Fibronectin and Collagen and Their Incorporation into the Extracellular Matrix*. OF BIOLOGICAL CHEMISTRY. 1986;261(9):4337–4345.
46. Lan Y, Liu B, Yao H, et al. Essential Role of Endothelial Smad4 in Vascular Remodeling and Integrity. Molecular and Cellular Biology. 2007;27(21):7683–7692. https://doi.org10.1128/mcb.00577-07. [PubMed: 17724086]
47. Sörensen I, Adams RH, Gossler A. DLL1-mediated Notch activation regulates endothelial identity in mouse fetal arteries. Blood. 2009;113(22):5680–5688. https://doi.org10.1182/blood-2008-08-174508. [PubMed: 19144989]
48. Phillips MT, Kirby ML, Forbes G. Analysis of Cranial Neural Crest Distribution in the Developing Heart Using Quail-Chick Chimeras. Circulation Research. 1987;60(1):27–30. https://doi.org10.1161/01.res.60.1.27. [PubMed: 3568286]
49. Miyagawa-Tomita S, Waldo K, Tomita H, Kirby ML. Temporospatial Study of the Migration and Distribution of Cardiac Neural Crest in Quail-Chick Chimeras The American Journal of Anatomy. 1991;192:79–88. https://doi.org10.1002/aja.1001920109. [PubMed: 1750383]
50. Creazzo TL, Godt RE, Leatherbury L, Conway SJ, Kirby ML. Role of cardiac neural crest cells in cardiovascular development. Annual Review of Physiology. 1998;60(1):267–286. https://doi.org10.1146/annurev.physiol.60.1.267.
51. McKenzie IA, Ohayon D, Li H, et al. Motor skill learning requires active central myelination. Science. 2014;346(6207):318–322. https://doi.org10.1126/science.1254960. [PubMed: 25324381]
52. Le Douarin NM, Teillet MAM. Experimental analysis of the migration and differentiation of neuroblasts of the autonomic nervous system and of neurectodermal mesenchymal derivatives, using a biological cell marking technique. Developmental Biology. 1974;41(1):162–184. https://doi.org10.1016/0012-1606(74)90291-7. [PubMed: 4140118]
53. Verberne ME, Gittenberger-de Groot AC, Van Iperen L, Poelmann RE. Distribution of different regions of cardiac neural crest in the extrinsic and the intrinsic cardiac nervous system. Developmental Dynamics. 2000;217(2):191–204. https://doi.org10.1002/(SICI)1097-0177(200002)217:2<191::AID-DVDY6>3.0.CO;2-X. [PubMed: 10706143]

54. Annese V, Navarro-Guerrero E, Rodríguez-Prieto I, Pardal R. Physiological Plasticity of Neural-Crest-Derived Stem Cells in the Adult Mammalian Carotid Body. Cell Reports. 2017;19(3):471–478. https://doi.org10.1016/j.celrep.2017.03.065. [PubMed: 28423311]
55. Bockman DE, Redmond ME, Waldo K, Davis H, Kirby ML. Effect of neural crest ablation on development of the heart and arch arteries in the chick. Am J Anat. 1987;180(4):332–341. https://doi.org10.1002/aja.1001800403. [PubMed: 3425561]
56. Porras D, Brown CB. Temporal-spatial ablation of neural crest in the mouse results in cardiovascular defects. Developmental Dynamics. 2008;237(1):153–162. https://doi.org10.1002/dvdy.21382. [PubMed: 18058916]
57. Rosenquist TH, Kirby ML, Van Mierop LHS. Solitary aortic arch artery. A result of surgical ablation of cardiac neural crest and nodose placode in the avian embryo. Circulation. 1989;80(5):1469–1475. https://doi.org10.1161/01.CIR.80.5.1469. [PubMed: 2805278]
58. Waldo KL, Kumiski D, Kirby ML. Cardiac neural crest is essential for the persistence rather than the formation of an arch artery. Developmental Dynamics. 1996;205(3):281–292. https://doi.org10.1002/(SICI)1097-0177(199603)205:3<281::AID-AJA8>3.0.CO;2-E. [PubMed: 8850564]
59. Sawada H, Rateri L. Debra., Moorleghen J. Jessica., Majesky W. Mark., Daugherty Alan. Smooth Muscle Cells Derived From Second Heart Field and Cardiac Neural Crest Reside in Spatially Distinct Domains in the Media of the Ascending Aorta—Brief Report. Arteriosclerosis, Thrombosis, and Vascular Biology. 2017;37(9):1722–1726. https://doi.org10.1161/ATVBAHA.117.309599. [PubMed: 28663257]
60. Waldo KL, Hutson MR, Ward CC, et al. Secondary heart field contributes myocardium and smooth muscle to the arterial pole of the developing heart. Dev Biol. May 1 2005;281(1):78–90. https://doi.org10.1016/j.ydbio.2005.02.012. [PubMed: 15848390]
61. Adachi N, Bilio M, Baldini A, Kelly RG. Cardiopharyngeal mesoderm origins of musculoskeletal and connective tissues in the mammalian pharynx. Development. Feb 3 2020;147(3). https://doi.org10.1242/dev.185256.
62. Verzi MP, McCulley DJ, De Val S, Dodou E, Black BL. The right ventricle, outflow tract, and ventricular septum comprise a restricted expression domain within the secondary/anterior heart field. Dev Biol. Nov 1 2005;287(1):134–45. https://doi.org10.1016/j.ydbio.2005.08.041. [PubMed: 16188249]
63. Hahn SA, Schutte M, Shamsul Hoque ATM, et al. DPC4, a candidate tumor suppressor gene at human chromosome 18q21.1. Science. 1996;271(5247):350–353. https://doi.org10.1126/science.271.5247.350. [PubMed: 8553070]
64. Kirby ML, Waldo KL. Role of neural crest in congenital heart disease. Circulation. 1990;82(2):332–340. https://doi.org10.1161/01.CIR.82.2.332. [PubMed: 2197017]
65. Kaartinen V, Dudas M, Nagy A, Sridurongrit S, Lu MM, Epstein JA. Cardiac outflow tract defects in mice lacking ALK2 in neural crest cells. Development. 2004;131(14):3481–3490. https://doi.org10.1242/dev.01214. [PubMed: 15226263]
66. Manderfield LJ, High FA, Engleka KA, et al. Notch activation of Jagged1 contributes to the assembly of the arterial wall. Circulation. 2012;125(2):314–323. https://doi.org10.1161/CIRCULATIONAHA.111.047159. [PubMed: 22147907]
67. Xie WB, Li Z, Shi N, et al. Smad2 and myocardin-related transcription factor B cooperatively regulate vascular smooth muscle differentiation from neural crest cells. Circulation Research. 2013;113(8):76–86. https://doi.org10.1161/CIRCRESAHA.113.301921.
68. Vermeiren S, Bellefroid EJ, Desiderio S. Vertebrate Sensory Ganglia: Common and Divergent Features of the Transcriptional Programs Generating Their Functional Specialization. Frontiers in Cell and Developmental Biology. 2020;8(October). https://doi.org10.3389/fcell.2020.587699.
69. Méndez-Maldonado K, Vega-López GA, Aybar MJ, Velasco I. Neurogenesis From Neural Crest Cells: Molecular Mechanisms in the Formation of Cranial Nerves and Ganglia. Frontiers in Cell and Developmental Biology. 2020;8(August). https://doi.org10.3389/fcell.2020.00635.
70. Harmon AW, Nakano Atsushi. Nkx2-5 Lineage Tracing Visualizes the Distributionof Second Heart Field-derived Aortic Smooth Muscle. Genesis 2013;51(12):862–869. https://doi.org10.1002/dvg.22721. [PubMed: 24133047]

71. Gittenberger-De Groot AC, DeRuiter MC, Bergwerff M, Poelmann RE. Smooth muscle cell origin and its relation to heterogeneity in development and disease. Arteriosclerosis, Thrombosis, and Vascular Biology. 1999;19(7):1589–1594. https://doi.org10.1161/01.atv.19.7.1589. [PubMed: 10397674]

72. Majesky MW. Developmental basis of vascular smooth muscle diversity. Arteriosclerosis, Thrombosis, and Vascular Biology. 2007;27(6):1248–1258. https://doi.org10.1161/ATVBAHA.107.141069. [PubMed: 17379839]

73. Gadson PF, Dalton ML, Patterson E, et al. Differential response of mesoderm- and neural crest-derived smooth muscle to TGF-β1: Regulation of c-myb and α1 (I) procollagen genes. Experimental Cell Research. 1997;230(2):169–180. https://doi.org10.1006/excr.1996.3398. [PubMed: 9024776]

74. Topouzis S, Majesky MW. Smooth muscle lineage diversity in the chick embryo. Two types of aortic smooth muscle cell differ in growth and receptor-mediated transcriptional responses to transforming growth factor-β. Developmental Biology. 1996;178(2):430–445. https://doi.org10.1006/dbio.1996.0229.

75. Leroux-Berger M, Queguiner I, MacIel TT, Ho A, Relaix F, Kempf H. Pathologic calcification of adult vascular smooth muscle cells differs on their crest or mesodermal embryonic origin. Journal of Bone and Mineral Research. 2011;26(7):1543–1553. https://doi.org10.1002/jbmr.382. [PubMed: 21425330]

76. Ruddy JM, Jones JA, Spinale FG, Ikonomidis JS. Regional heterogeneity within the aorta: Relevance to aneurysm disease. Journal of Thoracic and Cardiovascular Surgery. 2008;136(5):1123–1130. https://doi.org10.1016/j.jtcvs.2008.06.027. [PubMed: 19026791]

77. Sinha S, Iyer D, Granata A. Embryonic origins of human vascular smooth muscle cells: Implications for in vitro modeling and clinical application. Cellular and Molecular Life Sciences. 2014;71(12):2271–2288. https://doi.org10.1007/s00018-013-1554-3. [PubMed: 24442477]

78. Yang X, Li C, Herrera PL, Deng CX. Generation of Smad4/Dpc4 conditional knockout mice. Genesis. 2002;32(2):80–81. https://doi.org10.1002/gene.10029. [PubMed: 11857783]

79. Madisen L, Zwingman TA, Sunkin SM, et al. A robust and high-throughput Cre reporting and characterization system for the whole mouse brain. Nature Neuroscience. 2010;13(1):133–140. https://doi.org10.1038/nn.2467. [PubMed: 20023653]

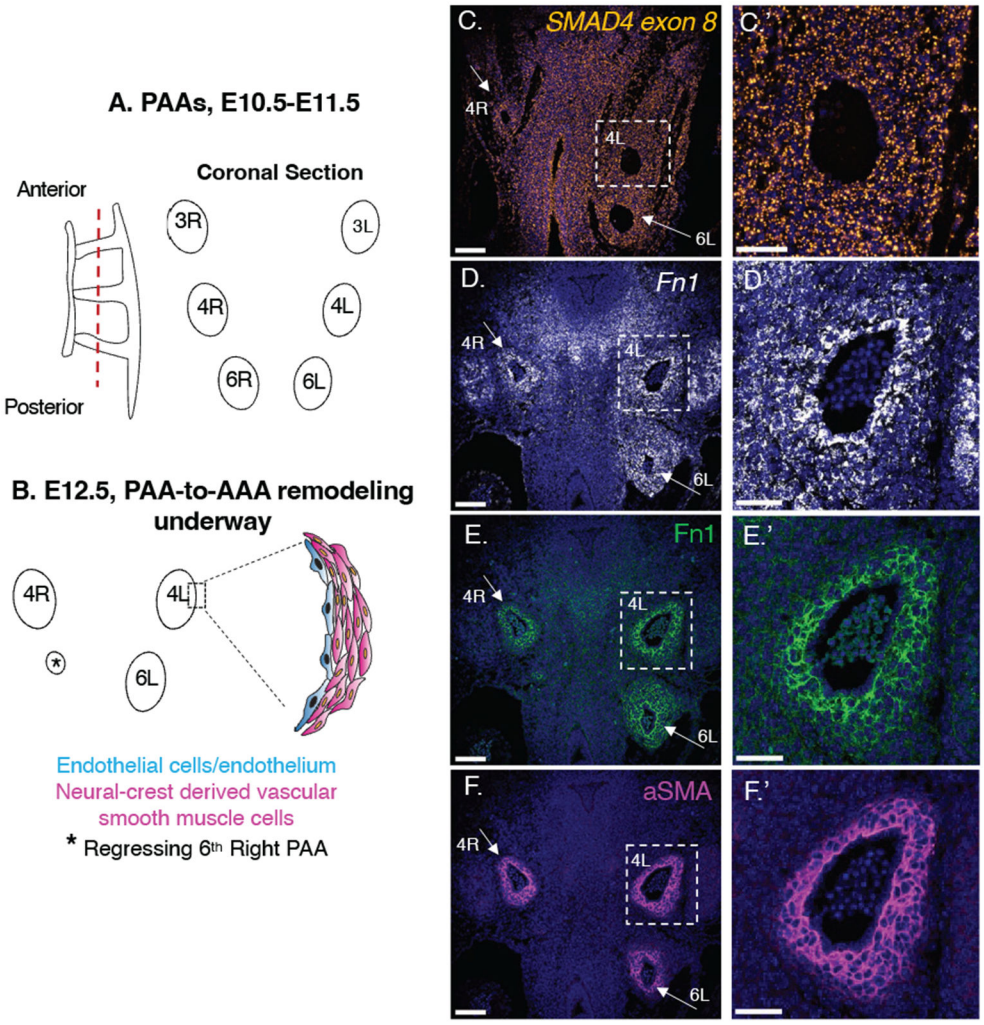

Figure 1. SMAD4 and Fn1 are highly expressed in the pharyngeal arches at E12.5.

A-B, Schematic depiction of PAAs at E10.5 – E12.5. The paired 3rd, 4th, and 6th PAAs (**A**) are remodeled between E11.5-E13.5 (**B**). The dashed red line in **(A)** indicates a coronal plane of section. Coronal sections through E12.5 PAs in a control embryo show expression of *SMAD4* mRNA (**C-C'**), *Fn1* mRNA (**D-D'**), Fn1 protein (**E-E'**), and αSMA (**F-F'**). White arrows point to the 4th right and 6th left PAAs. The 4th left pharyngeal arch (boxed) is magnified in **(C'-F')**. Scale bars in **C-F** are 100 μm. Scale bars in **C'- F'** are 50 μm.

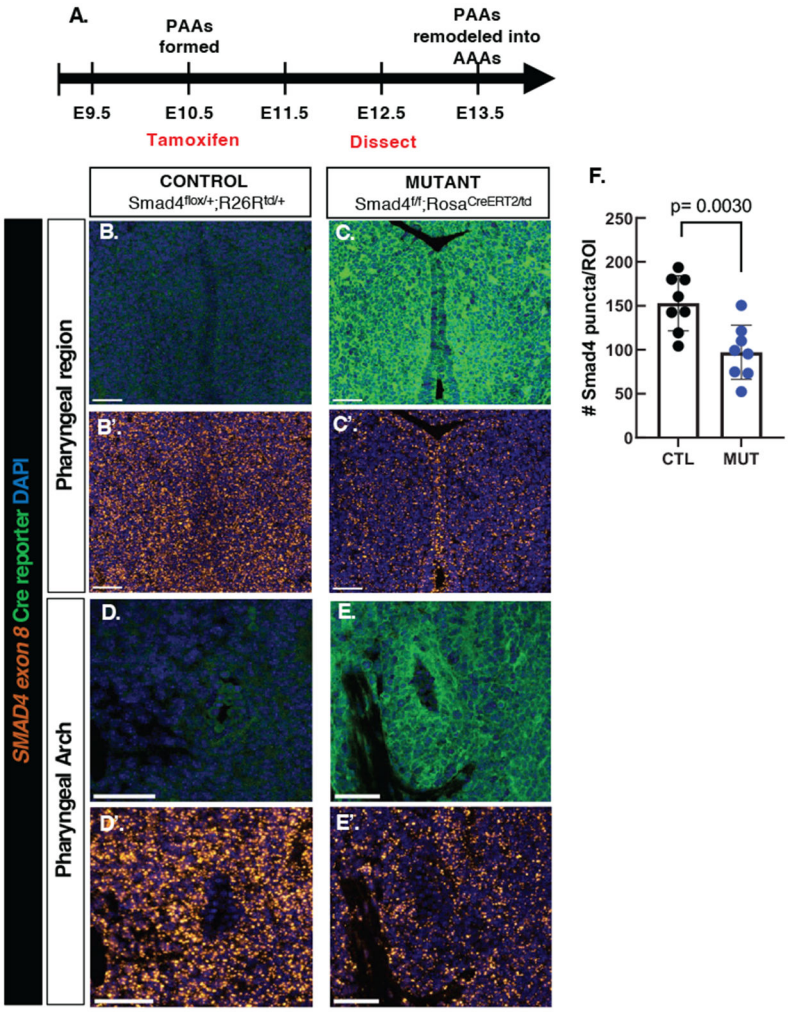

Figure 2. R26R^{CreERT2}-mediated recombination results in incomplete *SMAD4* knockdown.

(A) Experimental conditions. **B-E'** Images of *SMAD4* exon 8 fluorescence *in situ hybridization* and immunofluorescence for the Cre reporter in the pharyngeal region and pharyngeal arches of a controls (**B-B'**, **D-D'**), and mutants **(C-C'**, **E-E')**. 8 controls and 8 mutants were analyzed. **(F)**. Quantifications of *in situ* hybridization signal. Each data point is an average of 3 sections analyzed per embryo. 2-tailed, unpaired, Student's t-test was used; $p < 0.05$ was considered statistically significant. Scale bars are 50 μm.

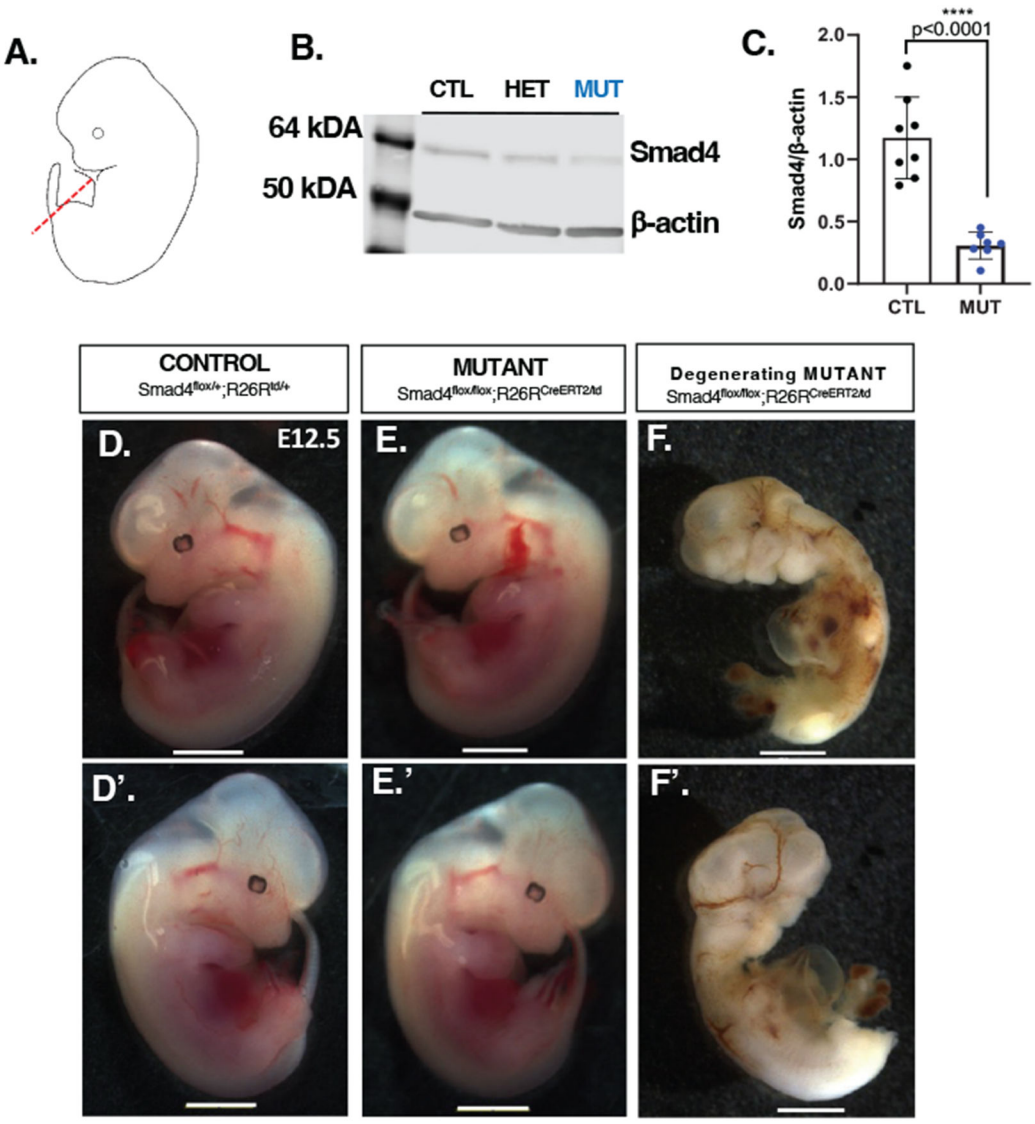

Figure 3.

Western blot analyses of E12.5 embryos from the cross between Smad4$^{flox/flox}$; R26R$^{Td/Td}$ females and Smad4$^{flox/+}$;R26R$^{CreERT2/Td}$ males. **A.** Schematic of posterior embryo region used for Western blot assays. **B.** Representative Western blot. CTL-control, Cre-negative, Smad4$^{flox/+}$ embryos; HET – heterozygous, Smad4$^{flox/+}$;R26R$^{CreERT2/Td}$ embryos, MUT – mutant, Smad4$^{flox/flox}$; R26R$^{CreERT2/Td}$ embryos. **C.** Quantifications of normalized SMAD4 protein expression levels in 8 controls and 7 mutants. Morphology of E12.5 embryos upon dissection **(D-F')**. Degenerating mutant **(F-F')** was not analyzed.

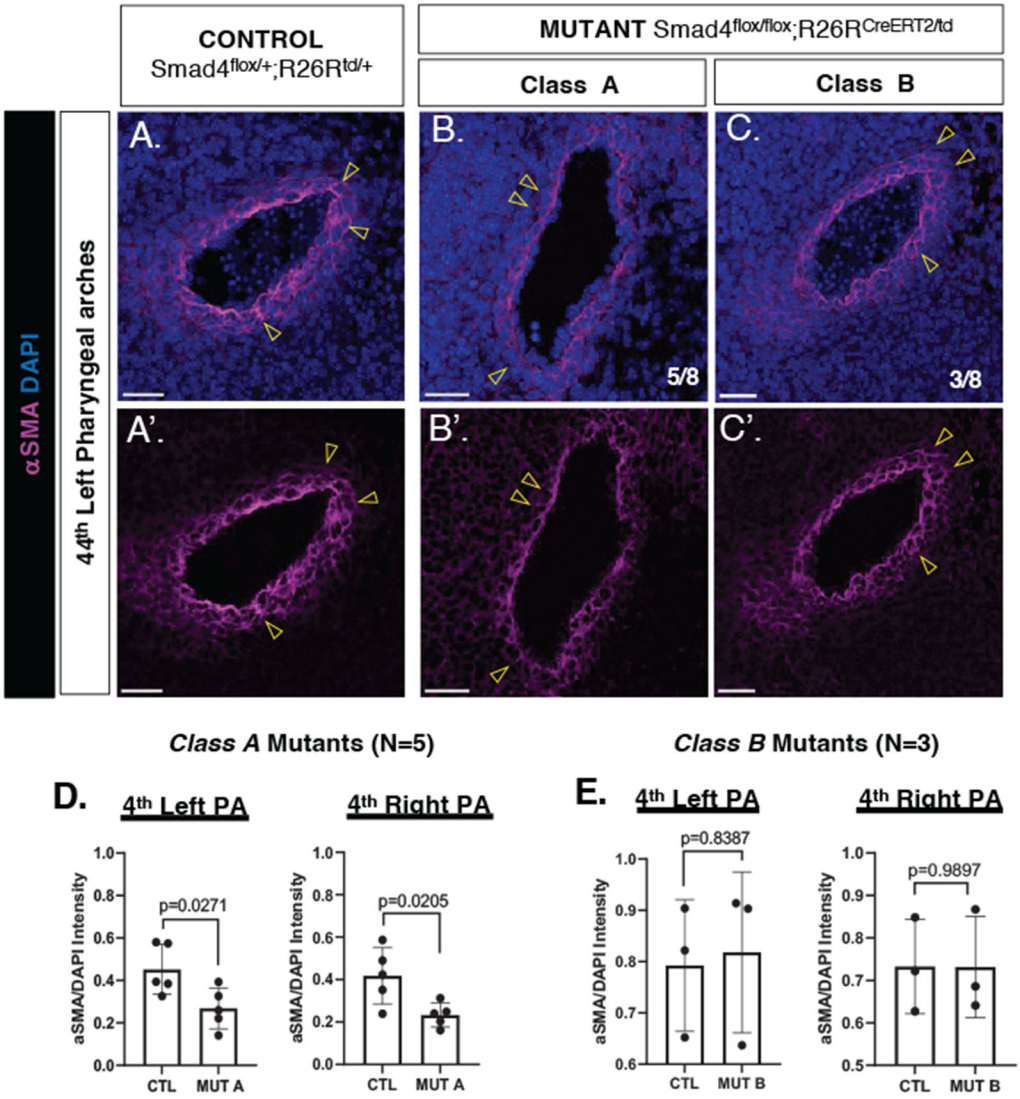

Figure 4. SMAD4 regulates smooth muscle differentiation.

Representative images of αSMA expression around the 4th PAA of controls (**A-A'**), and two classes of mutants **(B-B', C-C')**. Yellow arrowheads point to αSMA expression. (**D)** Quantifications of αSMA expression in *Class A mutants* (N=5), and (**E)** *Class B mutants* (N=3). A total of 8 controls and 8 mutants were analyzed for αSMA expression. Each data point is an average of 9-17 sections analyzed per embryo. 2-tailed, unpaired Student's t-tests were used for statistical analyses. Scale bars are 40 μm.

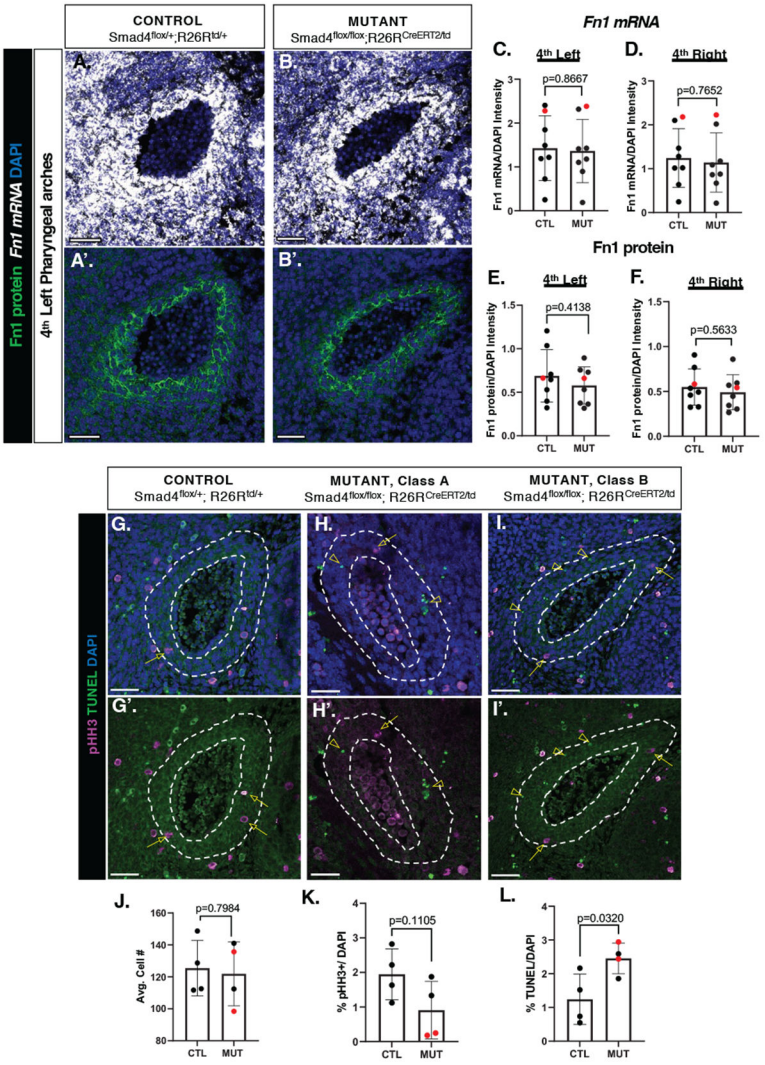

Figure 5. Global loss of SMAD4 does not attenuate fibronectin expression but marginally increases cell death around the pharyngeal arches.

Images of *Fn1 mRNA* and Fn1 protein expression on coronal sections through the 4th PAs in an E12.5 control (**A-A'**), and mutant (**B-B'**). Quantifications of *Fn1 mRNA* are shown in (**C-D**) and Fn1 protein shown in (**E-F**). 8 controls and 8 mutants were analyzed. Data points marked in red correspond with the IF images in **A-B'**. Each data point is an average of 9-17 sections analyzed per embryo. TUNEL and pHH3 staining were performed on consecutive control (**G-G'**) and mutant (**H-I'**) sections; arrows point to pHH3+ cells, and arrowheads point to TUNEL+ cells. Quantifications of average cell number, % pHH3+, and % TUNEL+ cells in 4-cell layers surrounding the PAA endothelium **(J-L) outlined** by the white dashed lines in (**G-I'**). Sections from 4 controls and 4 mutants were used for TUNEL and proliferation analyses. Mutants with decreased αSMA levels (Class A) marked in red. Each data point is an average of 3 sections analyzed per embryo. A 2-tailed, unpaired Student's t-test was used; Scale bars are 40 μm.

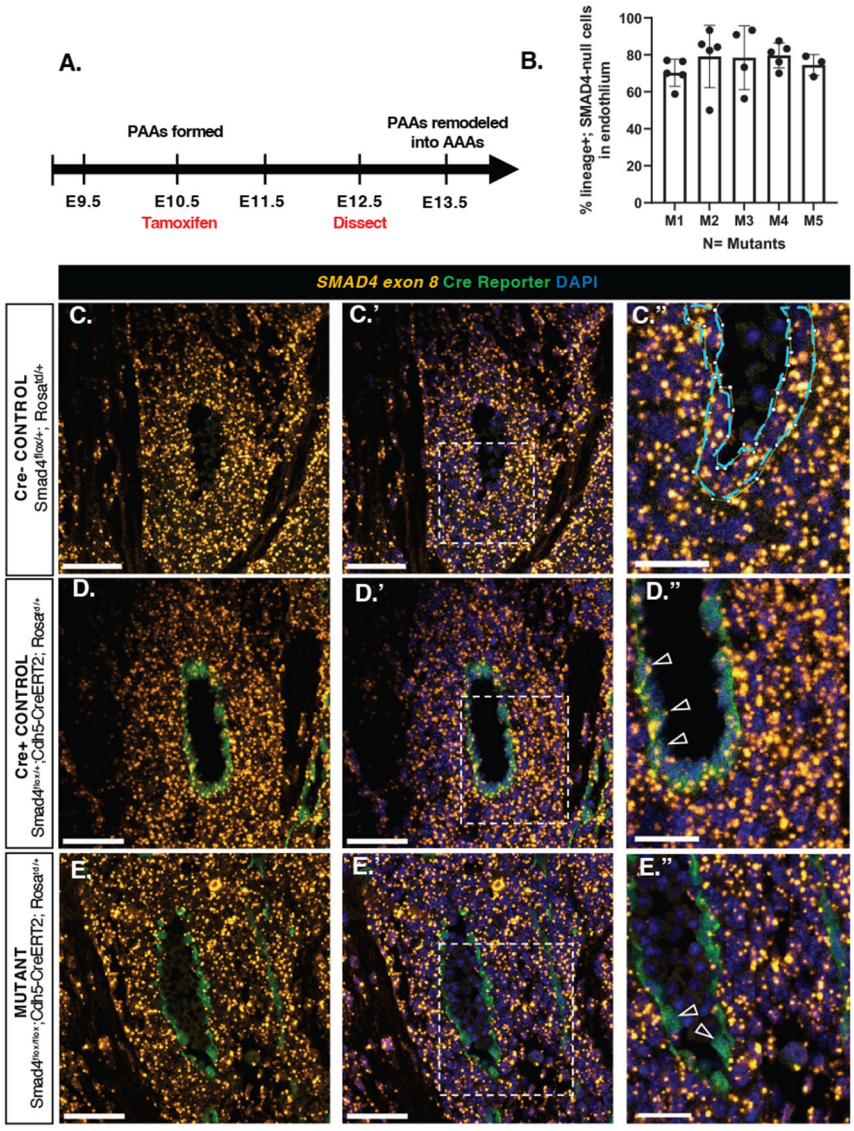

Figure 6. Cdh5-CreERT2-mediated SMAD4 loss is efficient in the PAA endothelium.

(**A**) Experimental conditions. (**B**) Percentage of Cdh5-lineage+; SMAD4-null cells were quantified in the PAA endothelium of five E12.5 mutants from 3 independent experiments. Representative images of fluorescence *in situ* hybridization for *SMAD4 exon 8 mRNA* and immunofluorescence for the Cre reporter in a Cre negative control (**C-C"**), Cre positive control (**D-D"**), and mutant (**E-E"**). Arrowheads point to Cre+; SMAD4+ cells in **D"** and Cre+; SMAD4-null cells in **E"**. Scale bars in **C-C', D-D'** and **E-E'** are 50 μm; scale bars in **C"**, **D"** and **E"** are 25 μm.

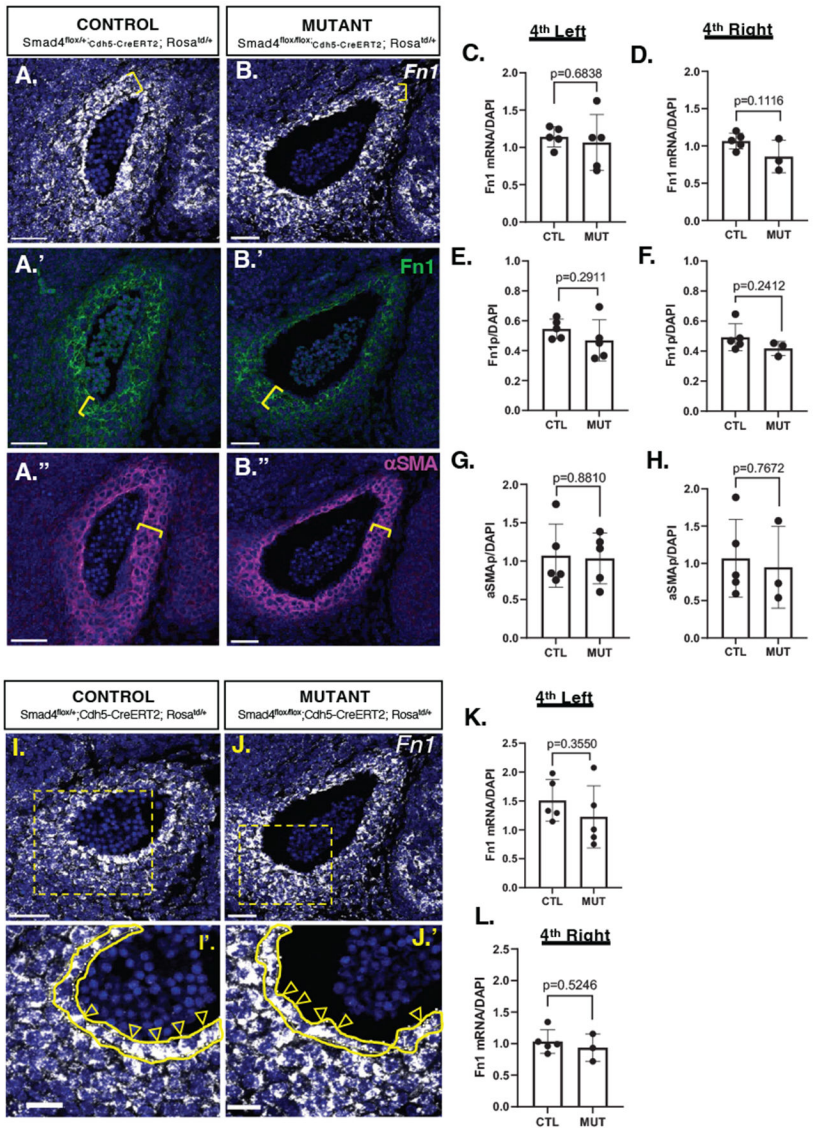

Figure 7. Endothelial loss of SMAD4 does not attenuate Fn1 or αSMA in the neural crest.

Images of fluorescent *in situ* hybridization for *Fn1* mRNA, immunofluorescence for Fn1 protein and αSMA in the 4th PAs of an E12.5 control (**A-A"**) and mutant (**B-B"**) embryo. NC-derived cell layers closest to the endothelium are indicated by yellow brackets. Quantifications of *Fn1* mRNA **(C-D)**, Fn1 protein **(E-F)**, and αSMA **(G-H)**. Images of *Fn1* mRNA in the PAA endothelium of a control (**I-I'**) and mutant **(J-J')** embryo. Yellow arrowheads indicate *Fn1* mRNA in the endothelium. Quantifications of *Fn1* mRNA in the endothelium (**K-L**). Left 4th PAs were analyzed in 5 controls and 5 mutants; Right 4th PAs were analyzed in 5 controls and 3 mutants. Each data point is an average of 5-20 sections analyzed per embryo. For statistics, a 2-tailed, unpaired Student's t-test was used; Scale bars in **A-J** are 50 μm and scale bars in **I'** and **J'** are 25 μm.

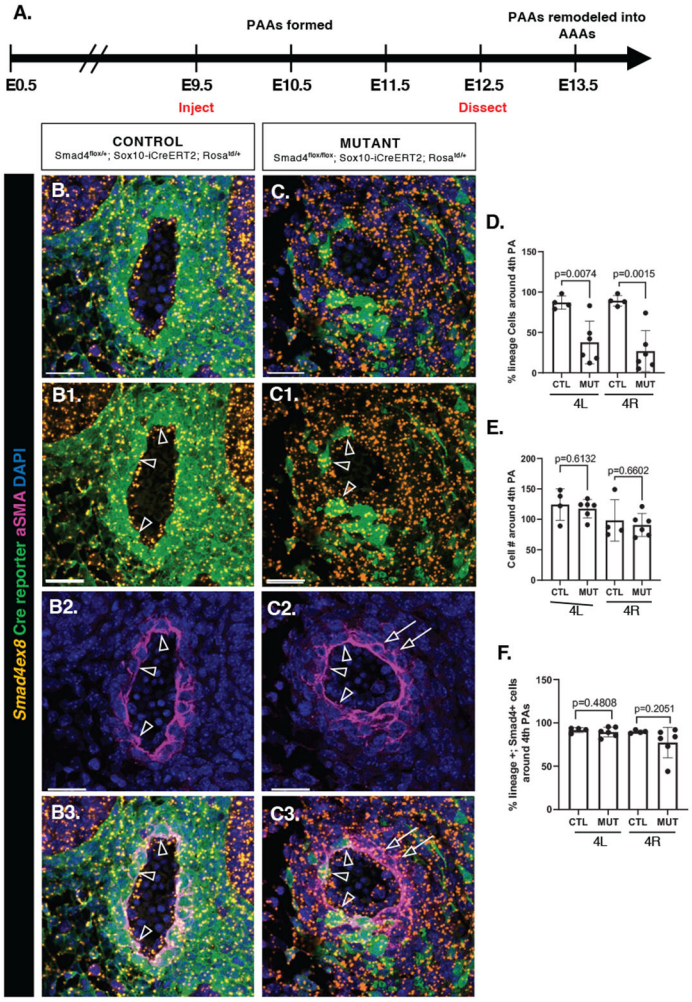

Figure 8. SMAD4 is required for neural crest contribution to the pharyngeal arches.

Experimental conditions (**A**). Fluorescent *in situ* hybridization for *SMAD4* exon 8 mRNA and immunofluorescence for the Cre reporter and αSMA on E12.5 coronal sections through the PAs of a control (**B-B3**) and mutant (**C-C3**) embryo. Arrowheads point to Cre+; SMAD4+ cells in the PAs that also express αSMA. Arrows in **C2-C3** point to lineage-negative cells, which express αSMA. Percent lineage cells within 4 cell layers closest to the endothelium quantified in (**D**). Total cell numbers in the same region are quantified in (**E**). Percent lineage cells expressing SMAD4 is quantified in (**F**). 4 controls and 6 mutants were examined Each data point is an average of 5-8 sections analyzed per embryo (**D-E**) and 2-3 sections per embryo in (**F**). Data was analyzed using a 2-tailed, unpaired Student's t-test; Scale bars are 50 μm.

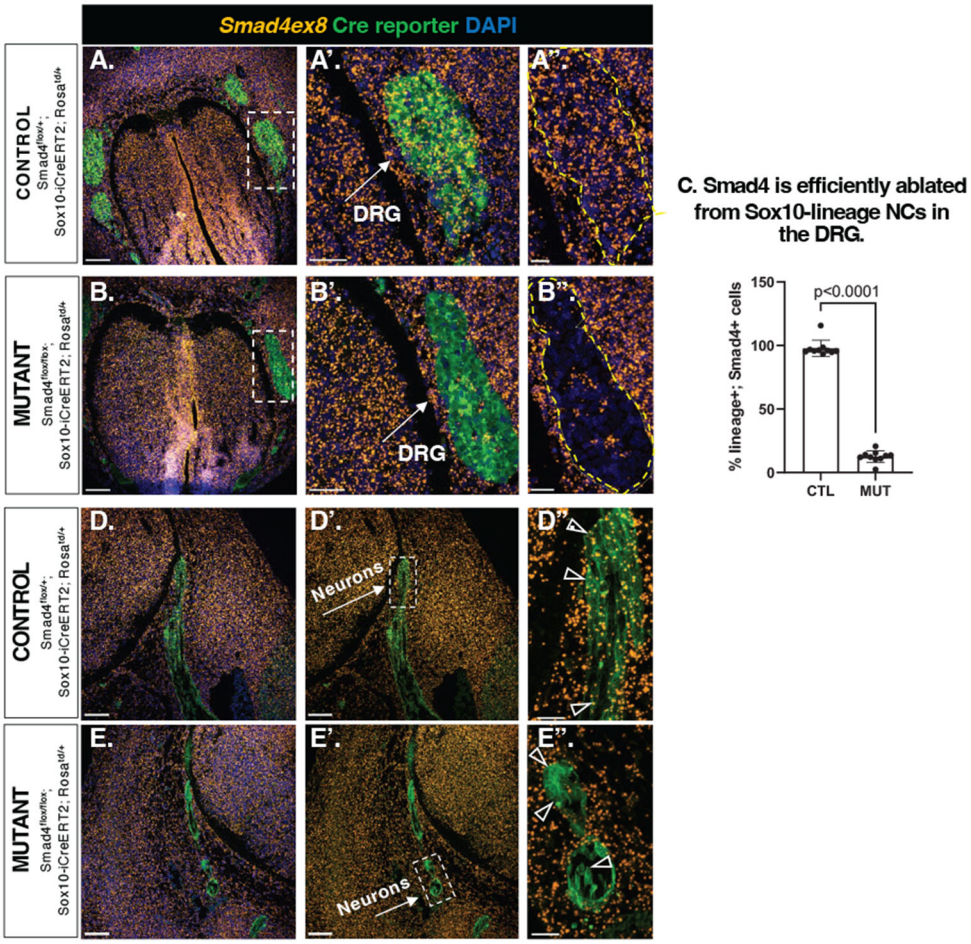

Figure 9. Sox10-iCreER^{T2} mediates efficient SMAD4 ablation in neural crest-lineage cells outside of pharyngeal arches.

Images of fluorescent *in situ* hybridization for *SMAD4 exon 8* mRNA and immunofluorescence for the Cre reporter on E12.5 coronal sections through the dorsal root ganglia (DRG) of a control (**A-A"**) and mutant (**B-B"**) embryo. Quantifications of the percentage of SMAD4+ Sox10-lineage cells in the DRGs (**C**). Each data point marks an individual section analyzed in 5 controls and 8 mutants. SMAD4 is also efficiently ablated in Sox10-lineage neurons (**D-E"**). Controls (**D-D"**) and mutants (**E-E"**). For statistics, a 2-tailed, unpaired, Student's t-test was used; Scale bars in **A-A', B-B', D-D', E-E'** are 100 μm and in **A"- E"** are 50 μm.

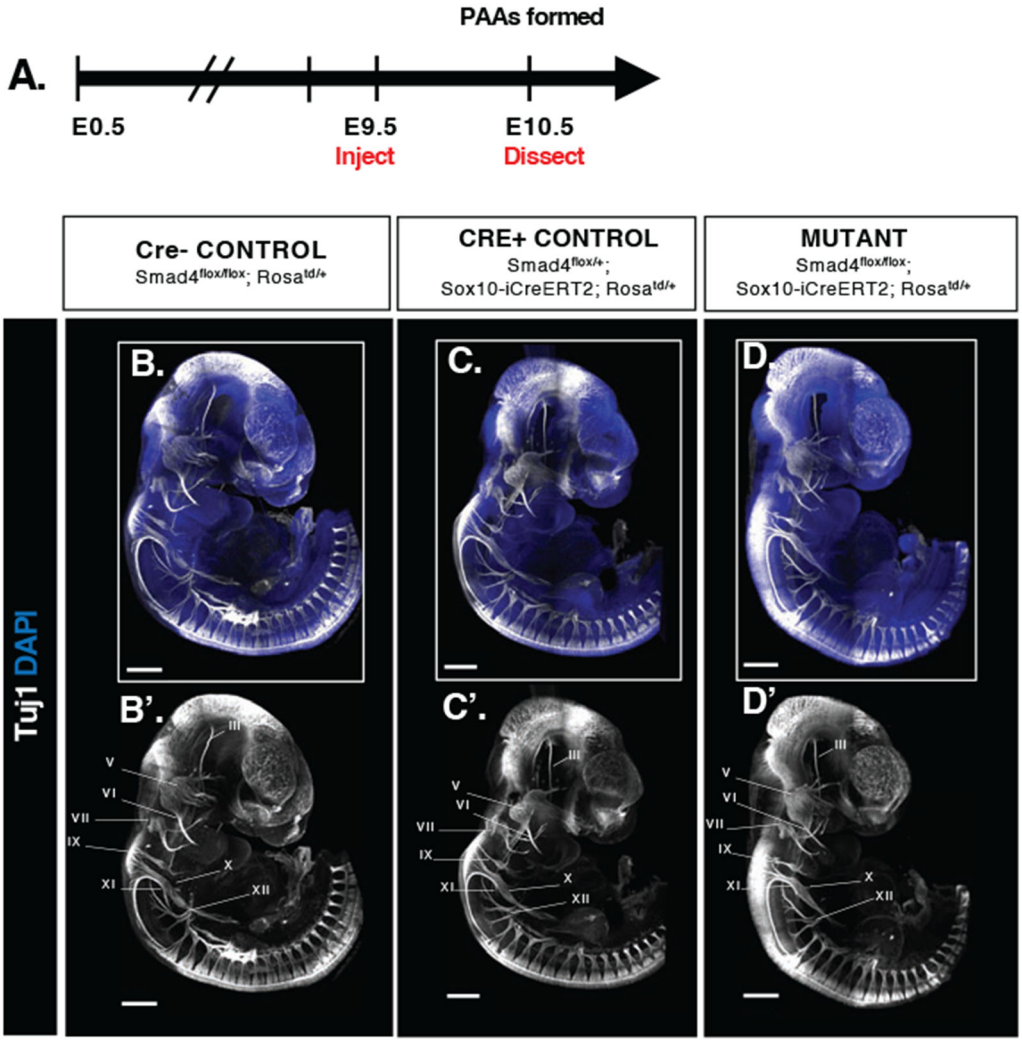

Figure 10. Loss of SMAD4 in the Sox10-lineage does not cause aberrant nerve patterning in E10.5 embryos.

A. Experimental timeline. Maximum intensity projection images of E10.5 embryos stained for the neuronal marker, Tuj1, in a Cre-negative control (**B-B'**), Cre-positive control (**C-C'**), and mutant embryo (**D-D'**). Cranial nerves are numbered with Roman numerals. Cre-negative control embryo 37 somites, Cre-positive Control embryo 37 somites, Mutant embryo 35 somites. Scale bars are 500 μm.

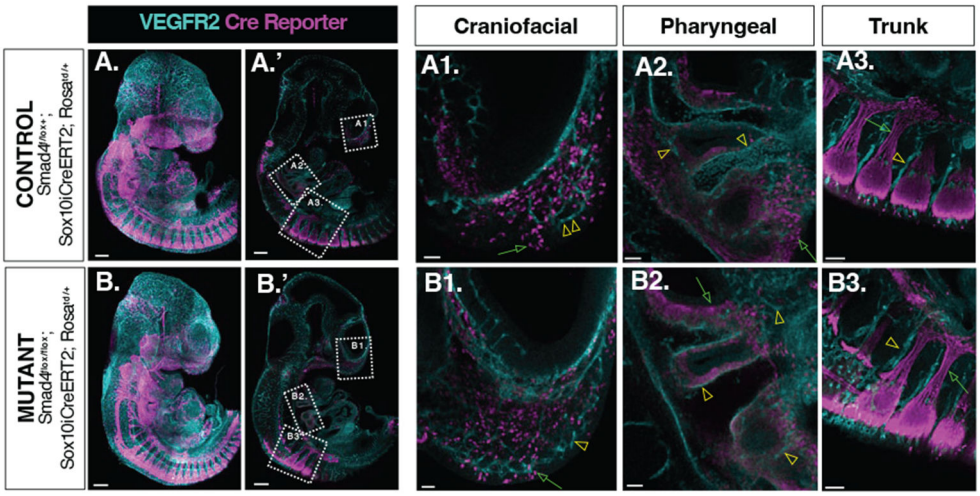

Figure 11. NC cells do not trans-differentiate to endothelial cells in Smad4$^{flox/flox}$;Sox10-iCreER^{T2} mutants.

Maximum intensity projection images of E10.5 embryos stained for the endothelial marker, VEGFR2, and the Cre reporter in control **(A-A3)** and mutant **(B-B3)** embryos. Boxed regions in **A'** and **B'** are magnified to show craniofacial **(A1, B1)**, pharyngeal **(A2, B2)**, and trunk **(A3, B3)** regions in the control and mutant embryo, respectively. Green arrows point to VEGFR2-negative, Sox10-lineage cells, and yellow arrowheads point to VEGFR2-positive, Sox10-lineage-negative endothelial cells. Scale bars are 300 μm in **A-A'** and **B-B'** and 50 μm in **A1-A3, B1-B3**. Cre+ Control embryo 37 somites, Mutant embryo 35 somites.

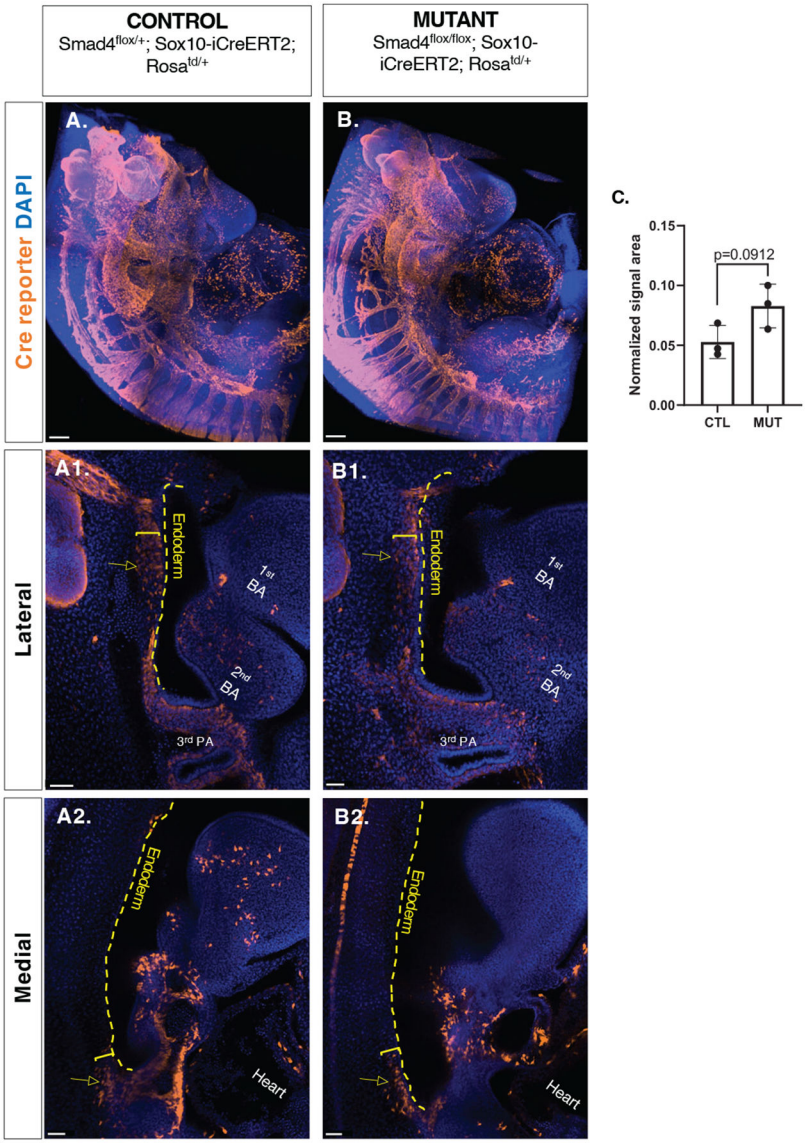

Figure 12. Neural crest contribution to the enteric nervous system in Smad4$^{flox/flox}$;Sox10-iCreER^{T2} embryos.

Maximum intensity projection images of E10.5 embryos stained for the Cre reporter in a control **(A-A2)** and mutant **(B-B2)** embryos. Lateral **(A1, B1)** and medial **(A2, B2)** slices through the endoderm are shown. The percentage of Sox10- lineage cells surrounding the endoderm is quantified in **(C)**. Each data point is an average of 5-13 sections analyzed in each embryo. 2-tailed, unpaired Student's t-test was used; 3 controls and 3 mutants were analyzed. Scale bars in **A-B** are 150 μm, and in **A1-B2** are 50 μm. The embryos shown are 35 somites.

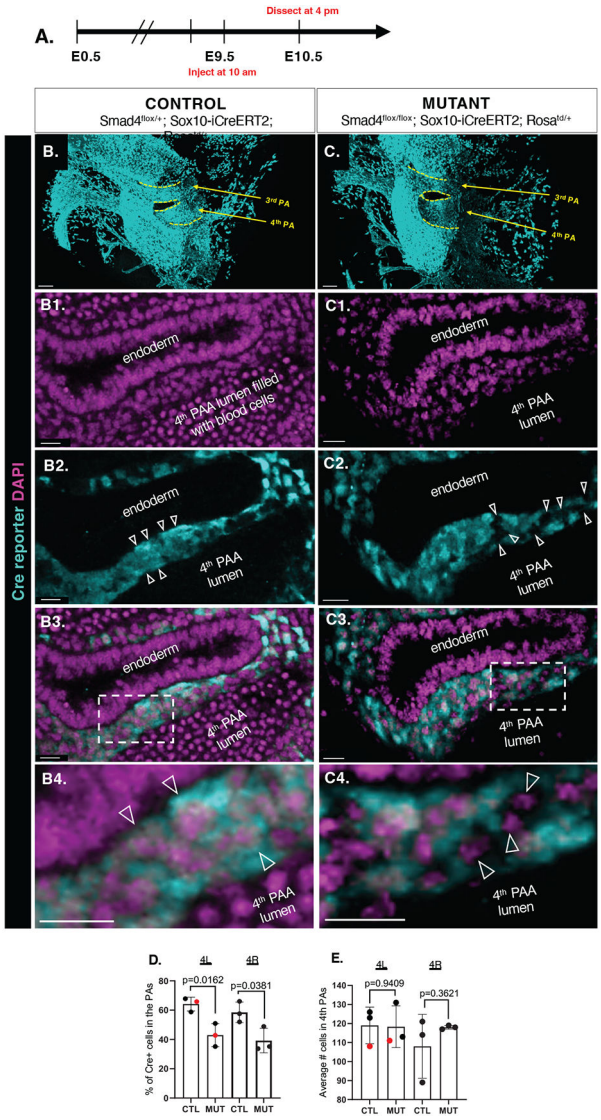

Figure 13. Smad4$^{flox/flox}$; Sox10-iCreER^{T2} mutants have reduced numbers of neural crest-lineage cells in the PAs at E10.5.

(A) Experimental conditions. Maximum intensity projection of the pharyngeal regions from E10.5 embryos stained for the Cre reporter in a Cre+ control **(B, B1-B4)** and mutant **(C, C1-C4)** embryo. Dashed yellow lines in **(B, C)** outline pharyngeal arches. White arrowheads indicate Sox10-lineage cells in the control **(B2, B4)** and non-Sox10-lineage cells in the mutant **(C2, C4)**. Boxed regions in **(B3-C3)** are magnified in **(B4-C4)**. Percent Cre+ Sox10 lineage cells in 4th left and 4th right PAs are quantified in **(D)**. Average number of cells in 4th left and 4th right PAs quantified in **(E)**. 2-tailed, unpaired Student's t-test was used; 3 control and 3 mutants were analyzed. Each data point is an average of 4 – 6 sections analyzed in each embryo. Analyzed sections were spaced 10 μm apart. Scale bars in **A-B** are 100 μm; all other scale bars are 20 μm. The embryos shown are 35 somites. Data points in red correspond with samples shown in **B-C**.

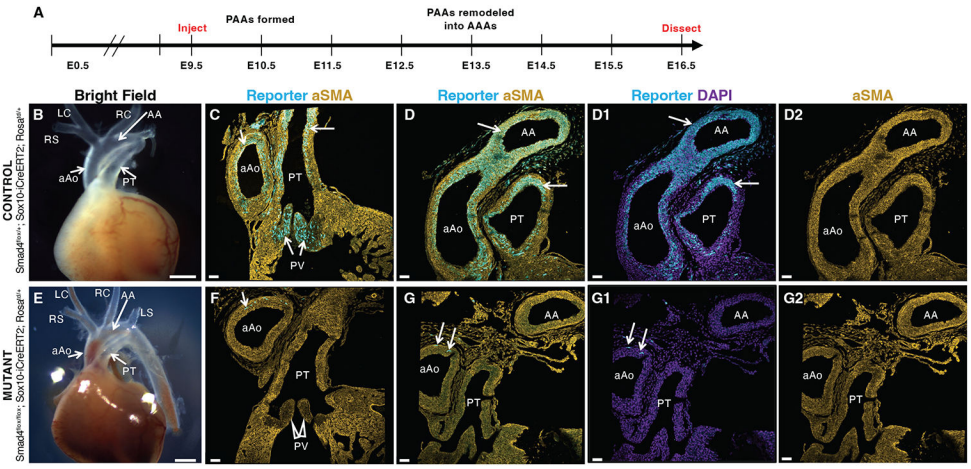

Figure 14. Alternative cellular source compensates for the absent neural crest-derived cells and mediates proper arch artery morphogenesis and smooth muscle differentiation in Smad4$^{flox/flox}$; Sox10-iCreER^{T2} mutants at E16.5.

A. Experimental timeline. 8 control and 4 mutant embryos were analyzed from three litters. **B-D2.** Control and **E-G2.** Mutant. **B, E.** Bright field images of dissected hearts and vasculature. aAo-ascending aorta, PT-pulmonary trunk, RS and LS – right and left subclavian arteries, RC and LC – right and left carotid arteries. **C-D2** and **F-G2** – coronal paraffin sections through the heart and the vasculature. Arrows point to NC-derived cells. Arrowheads in **F** point to the pulmonary valve (PV) in the mutant. Note the presence of abundant NC-derived cells (cyan) in pulmonary valves, distal ascending aorta, pulmonary trunk, and the aortic arch in controls (**C-D2**). There are only rare NC-derived cells present in the vSMC coat of mutants (arrows in **F-G1**). The majority of αSMA+ (orange) cells in the mutants are derived from an alternative source. Scale bars in B and E are 1 mm, and scale bars **in C-D2** and **E-G2** are 50 μm.

Table 1:

Frequency of genotypes among harvested E12.5 R26R-lineage embryos.

Cross $Smad4^{flox/flox}$; $R26R^{td/td}$ x $Smad^{flox/+}$; $R26R^{CreERT2}$		Control $Smad4^{flox/flox}$;$R26R^{td/+}$ OR $Smad4^{flox/+}$;$R26R^{td/+}$	Heterozygous $Smad4^{flox/+}$;$R26R^{td/CreERT2}$	Mutant $Smad4^{flox/flox}$;$R26R^{td/CreERT2}$	Total N	χ^2
Observed	E12.5	79 (48.2%)	38 (23.2%)	*47 (28.6%)	164	0.614
Expected		82 (50%)	41 (25%)	41 (25%)		

*One embryo was grossly defective (Fig. 3F-F') and, thus, not used for analyses.

Table 2:

Detailed list of commercially available strains used in this study.

Strain Name	Stock No.	Reference	Manuscript shorthand
Smad4$^{tm2.1cxd}$/J	**017462**	Yang et al., 2002	Smad4$^{flox/flox}$
B6.129-Gt(ROSA)26Sortm1(cre/ERT2)Tyj/J	**008463**	Ventura et al., 2007	R26R^{CreERT2}
CBA;B6-Tg(Sox10-icre/ERT2)388Wdr/J	**027651**	McKenzie et al., 2014	Sox10-iCreER^{T2}
B6.Cg-Gt(ROSA)26Sortm9(CAG-tdTomato)Hze/J	**007909**	Madisen et al., 2010	R26R$^{Td/Td}$

Table 3.

Links to external protocols referenced.

Prot. #	Prot. name	Link
1	TUNEL	https://www.sigmaaldrich.com/deepweb/assets/sigmaaldrich/product/documents/419/175/11684795910.pdf
2	Fluorescent Multiplex	https://acdbio.com/sites/default/files/UM%20323100%20Multiplex%20Fluorescent%20v2_RevB.pdf
3	Multiplex + IHC	https://acdbio.com/sites/default/files/323100-TN%20Multiplex%20Fluorescent%20V2%20with%20IF_incOpal780.pdf
4	Basescope RED + IHC	https://acdbio.showpad.com/share/3eLIrIP9sGPnD5pYCshq2

Protocols listed in Table 3 were used without modifications.